Title
A Dramatic Increase of C1q Protein in the CNS during Normal Aging

Journal
Journal of Neuroscience, 33(33)

ISSN
0270-6474

Authors
Stephan, Alexander H
Madison, Daniel V
Mateos, José María
et al.

Publication Date
2013-08-14

DOI
10.1523/jneurosci.1333-13.2013

Peer reviewed

Development/Plasticity/Repair

A Dramatic Increase of C1q Protein in the CNS during Normal Aging

Alexander H. Stephan,[1] Daniel V. Madison,[2] José María Mateos,[3] Deborah A. Fraser,[4] Emilie A. Lovelett,[1] Laurence Coutellier,[5] Leo Kim,[5] Hui-Hsin Tsai,[6,7,8] Eric J. Huang,[9] David H. Rowitch,[6,7,8] Dominic S. Berns,[1] Andrea J. Tenner,[4] Mehrdad Shamloo,[5] and Ben A. Barres[1]

Stanford University School of Medicine, Departments of [1]Neurobiology and [2]Molecular and Cellular Physiology, Stanford, California 94305-5345, [3]Center for Microscopy and Image Analysis, University of Zurich, 8057 Zurich, Switzerland, [4]Departments of Molecular Biology and Biochemistry, Neurobiology and Behavior, and Pathology and Laboratory Medicine, University of California, Irvine, California 92697-3900, [5]Behavioral and Functional Neuroscience Laboratory, Stanford University School of Medicine, Stanford, California 94305-5345, [6]Howard Hughes Medical Institute, [7]Department of Pediatrics, [8]Eli and Edythe Broad Center of Regeneration Medicine and Stem Cell Research, and [9]Department of Pathology, University of California San Francisco, San Francisco, California 94143-0734

The decline of cognitive function has emerged as one of the greatest health threats of old age. Age-related cognitive decline is caused by an impacted neuronal circuitry, yet the molecular mechanisms responsible are unknown. C1q, the initiating protein of the classical complement cascade and powerful effector of the peripheral immune response, mediates synapse elimination in the developing CNS. Here we show that C1q protein levels dramatically increase in the normal aging mouse and human brain, by as much as 300-fold. This increase was predominantly localized in close proximity to synapses and occurred earliest and most dramatically in certain regions of the brain, including some but not all regions known to be selectively vulnerable in neurodegenerative diseases, i.e., the hippocampus, substantia nigra, and piriform cortex. C1q-deficient mice exhibited enhanced synaptic plasticity in the adult and reorganization of the circuitry in the aging hippocampal dentate gyrus. Moreover, aged C1q-deficient mice exhibited significantly less cognitive and memory decline in certain hippocampus-dependent behavior tests compared with their wild-type littermates. Unlike in the developing CNS, the complement cascade effector C3 was only present at very low levels in the adult and aging brain. In addition, the aging-dependent effect of C1q on the hippocampal circuitry was independent of C3 and unaccompanied by detectable synapse loss, providing evidence for a novel, complement- and synapse elimination-independent role for C1q in CNS aging.

Introduction

Cognitive decline is one of the greatest health threats for the aging population (Bishop et al., 2010) and is caused by synaptic malfunction and/or synapse loss, rather than the loss of neurons per se (Yankner et al., 2008). The molecular mechanisms driving cognitive aging, in particular the ones that drive the synaptic changes are, however, unknown. Rapidly growing evidence implicates molecules formerly believed to exclusively serve immune functions in a wide variety of CNS functions (Boulanger, 2009; Elmer and McAllister, 2012; Stephan et al., 2012). For instance, the classical complement cascade, initiated by the pattern-recognition molecule C1q, which is a powerful effector of the innate immune system and responsible for pathogen targeting and removal (Ricklin et al., 2010). We recently found that C1q helps to mediate developmental CNS synapse elimination through classical complement activation which is crucial for fine-tuning the visual system circuitry (Stevens et al., 2007). Furthermore, C1q was shown to also act independently of classical complement, contributing to neuroprotection in the CNS (Benoit and Tenner, 2011; Benoit et al., 2013).

As C1q and the classical complement cascade are strongly activated in Alzheimer's disease (Stephan et al., 2012), a disease of old age that is marked by massive synapse loss, here we investigated whether C1q also plays a role in the cognitive decline of normal brain aging.

Materials and Methods

Animals. C1q-deficient mice were generated by homologous recombination targeting exon 1 of the *C1q(a)* gene (Botto et al., 1998) and backcrossed for >10 generations to C57BL/6. *C1q(a)*-deficient mice

Received March 29, 2013; revised May 26, 2013; accepted July 15, 2013.

Author contributions: A.H.S., D.V.M., J.M.M., L.C., and B.A.B. designed research; A.H.S., D.V.M., J.M.M., E.A.L., L.K., H.-H.T., E.J.H., D.H.R., and D.S.B. performed research; D.A.F. and A.J.T. contributed unpublished reagents/analytic tools; A.H.S., D.V.M., J.M.M., E.A.L., L.C., L.K., and M.S. analyzed data; A.H.S. and B.A.B. wrote the paper.

This work was supported by funding from the Swiss National Science Foundation (A.H.S.), NIH RO1 DA15403 (B.A.B.), Fidelity Biosciences Research Initiative and Myelin Repair Foundation (B.A.B.), Senior Scholar Award in Aging from the Ellison Medical Foundation (B.A.B.), NIMH MH65541 (D.V.M.), The G. Harold and Leila Y. Mathers Charitable Foundation (D.V.M.), NIH NS059893 (D.H.R. and B.A.B.), NIH OD010927, University of California Pediatric Neuropathology Consortium and MRPI (E.J.H.); NIH AG00538 and AI41090 (A.J.T.). D.H.R. is a Howard Hughes Medical Institute Investigator. We thank Andrew Olson (Stanford Neuroscience Microscopy Service, supported by NIH NS069375) for microscopy support, Nay Lui Saw and Zhengqiu Shirrly Zhou for assisting the behavioral analysis (NIH NS069375), Rong Mao and Tirin Moore for advice on physiology data analysis, Kristin L. Sainani for statistics advice, Bruno Guhl and Gery Barmettler for electron microscopy support, and Vincent and Stella Coates for their generous support.

B.A.B. is a cofounder of Annexon, Inc., a new company that will develop therapeutics for neurological diseases.

Correspondence should be addressed to Dr Alexander Stephan, Stanford University, 299 Campus Drive MC5125, Fairchild Science Building D205, Stanford, CA 94305-5125. E-mail: astephan@stanford.edu or alexander_h_stephan@hotmail.com.

D. A. Fraser's present address: Department of Biological Sciences, California State University at Long Beach, 1250 Bellflower Boulevard, Long Beach, CA 90840-9502.

DOI:10.1523/JNEUROSCI.1333-13.2013

 0270-6474/13/3313460-15$15.00/0

(C57BL/6) have no C1q protein and disrupted classical complement activity (Botto et al., 1998). C3-deficient mice (C57BL/6), generated by homologous recombination targeting the coding sequence (nt 1850–2214) of the *C3* gene, were obtained from The Jackson Laboratory (B6 129S4-*C3*<*tmCrr*>/J; stock No. 003641). Young C57BL/6 mice, including the C57BL/6 mice used as strain-matched control for behavioral assays, were obtained from Charles Rivers Laboratories, and aged C57BL/6 mice were obtained from the National Institute on Aging. *Cx3CR1-GFP* knock-in mice (The Jackson Laboratory; B6.129P-*Cx3cr1*^{tm1Litt}/J, stock No. 005582) were crossed with C57BL/6 mice to maintain the line and to obtain heterozygous mice (*Cx3CR1-GFP*$^{+/-}$) used in the analyses presented. Animals were housed under pathogen-free conditions and handled according to laboratory animal care program (APLAC) guidelines at Stanford University, based on the National Institutes of Health *Guide for the Care and Use of Laboratory Animals*. Genotypes of all transgenic, knock-in or knock-out mice used were confirmed before and after experiments by PCR genotyping.

Human tissue. Brain specimens from both infant and aged donors were removed during autopsy and hippocampal tissues (at the level of lateral geniculate nucleus) were dissected by a neuropathologist. All specimens were collected with permits and in accordance with the University of California San Francisco Committee on Human Research. Tissue blocks were immersed in 4% (w/v) paraformaldehyde (PFA) in PBS for 48 h at 4°C. The tissues were then cryoprotected sequentially by 10 and 30% (w/v) sucrose in PBS at 4°C. After cryoprotection, tissues were embedded in OCT and cut at 12 μm thickness. Sections were stored at −80°C until use.

Rabbit anti-mouse C1q monoclonal antibody production. Mouse C1q was purified from normal mouse serum (Genetex) as previously described (Li et al., 2008), with the following additions. After purification by ion exchange chromatography (BioRex70, Bio-Rad) and before the affinity chromatography step (heparin-agarose, Bio-Rad), concentrated mouse C1q was applied to a size-exclusion chromatography column (sepharose 6B, GE Healthcare) equilibrated with 50 mM Tris pH 7.3, 400 mM NaCl, 25 mM EDTA. Fractions positive for C1q by hemolytic titer were pooled, concentrated by ultrafiltration, and buffer was exchanged into 50 mM Tris pH 7.3, 150 mM NaCl.

Immunization of rabbits with purified mouse C1q and subsequent cloning of anti-C1q antibody producing hybridoma cells was done by Epitomics. Antibody-producing hybridoma clones were further selected by ELISA screening and individual antibody clones were further selected and characterized by SDS-PAGE and immunohistochemistry.

Mouse perfusion. Mice were anesthetized with ketamine/xylazine and transcardially perfused with Dulbeccos PBS (Invitrogen) according to APLAC guidelines at Stanford University, based on the NIH *Guide for the Care and Use of Laboratory Animals*, until tissue was completely cleared of blood traces. If tissue fixation was required, the animals were additionally perfused with 10 ml 4% PFA/PBS solution. Mice were decapitated immediately after perfusion and brain tissue was carefully extracted and further processed (see below).

Immunohistochemistry staining and data analysis. Perfusion-fixed brains were additionally immersion-fixed with 4% PFA for 3 or 16 h at 4°C, dependent on the individual experimental requirements. The fixed brains were briefly rinsed in PBS before sunken in 30% sucrose/PBS solution at 4°C. Subsequently, 30 μm sections were produced with a freezing-sliding microtome and stored in PBS including 0.05% NaN_3 at 4°C. For immunohistochemistry analysis, sections were blocked in sterile-filtered antibody buffer (150 mM NaCl, 50 mM Tris base, 1% BSA, 100 mM L-lysine, 0.2% TX-100, pH 7.4) containing additional 2% BSA for 45 min and then transferred into primary antibody-containing antibody buffer for overnight to 3 d incubation at 4°C. Primary antibodies used: rabbit anti-mouse C1q monoclonal antibody (clones 4.8 and 27.10 at 1.0 μg/ml, Epitomics/Abcam), rabbit anti-human C1q (1:1000, Dako), mouse anti-synaptophysin (1:1000, Millipore), mouse anti-gephyrin (1:500, Synaptic Systems), guinea-pig anti-VGluT1 (1:1000, Millipore), guinea-pig anti-VGAT (1:250, Synaptic Systems), guinea-pig anti-GABA (1:500, abcam), mouse anti-NeuN (1:500, Millipore), chicken anti-GFP (1:1000, Abcam). After several washes in PBS, sections were incubated with adequate fluorescence-conjugated secondary antibodies (Jackson ImmunoResearch) for 2 h to overnight at room temperature in darkness. After washing with PBS, sections were mounted on glass slides, using VectaShield mounting medium (Vector Laboratories) and 0.17 mm thick glass coverslips. Stained tissue was subsequently analyzed with a Zeiss AxioImager wide field microscope or a Zeiss LSM 710 confocal microscope. Images from C1q-deficient and wild-type littermate mice, as well as tissue analyzed for the time course series were recorded under identical conditions and were postprocessed with Photoshop (Adobe) with identical settings. Signal quantification was performed with ImageJ 1.47f (NIH) on unprocessed image sections. Significance was determined with GraphPad Prism 5 using unpaired (see Figs. 1, 3, and 6) or paired (see Fig. 4), two-tailed *t* tests.

Tissue preparation for Western blotting. Perfused mouse brains or human hippocampal samples were homogenized on ice in sample buffer (50 mM HEPES, 5 mM $CaCl_2$, 1 mM $MgCl_2$, 145 mM NaCl, pH 7.4) containing protease inhibitor cocktails (Sigma). If required, mouse hippocampi were dissected in ice-cold PBS, homogenized and lysed for 1 h in sample buffer, containing 0.5% NP-40 (Pierce) at 4°C. Large debris was removed by centrifugation at 1000 × *g* for 5 min and supernatant samples were snap-frozen in liquid nitrogen, and stored at −80°C until use.

Crude synaptosomal preparation. Crude synaptosomes were prepared as described by Stephan et al. (2008). In brief, isolated hippocampi were homogenized with a glass-Teflon homogenizer (800 rpm, 12 strokes) in synaptosome buffer (320 mM sucrose, protease inhibitors, in 5 mM HEPES, pH 7.5) and centrifuged at 1000 × *g* for 5 min. The resulting supernatant was further centrifuged at 12,000 × *g* for 20 min to produce the crude synaptosomal pellet (P2) and synapse-free supernatant fraction (S2). The P2 was resuspended in buffer and both S2 and P2 were snap-frozen in liquid nitrogen, and stored at −80°C until Western blot analysis.

SDS-PAGE, Western blotting, and signal quantification. Protein concentrations were determined by Bradford protein assay (Bio-Rad) and SDS samples were prepared with standard Laemmli buffer. Dependent on tissue and antibody used, 15–35 μg of protein were loaded onto 4–15% TGX precast gels (Bio-Rad), separated by SDS-PAGE and subsequently transferred to polyvinylidene fluorid membranes (Immobilon P membrane, Millipore), according to the manufacturer's guidelines. The membranes were dried and then incubated with primary antibodies in Tris-buffered saline containing 0.1% Tween 20 (TBST) and 2.5% Western blocking reagent (Roche) for 90 min at room temperature. Primary antibodies used: goat anti-mouse C1q (1:50, Santa Cruz Biotechnology), goat anti-mouse C3 (1:1000, MP Biomedical), rabbit anti-PSD-95 (1:250, Invitrogen), goat anti-mouse IgG/IgM (1 μg/ml, Jackson ImmunoResearch), mouse anti-β-actin (1:2000, Abcam), mouse anti-β-tubulin (1:2000, Abcam), rabbit anti-GAPDH (1:2000, Abcam). After washing with TBST, the blots were incubated for 45 min with peroxidase-conjugated secondary antibodies (Jackson ImmunoResearch), and washed again. Immunoreactive protein bands were detected using the ECL-plus kit (GE Healthcare). Signals were acquired using a FluorChemQ CCD system (ProteinSimple) and analyzed using the manufacturer's software. For reprobing, membranes were incubated for 20 min in stripping solution (Pierce) and were afterward extensively washed in TBST before incubation with primary antibodies. For Western blot quantifications, signal intensities of proteins from at least three different animals per genotype or age were normalized to the β-tubulin or β-actin loading control for each individual sample and significance was determined with GraphPad Prism 5 using unpaired, two-tailed *t* test.

Histology (Golgi analysis). Golgi staining of mouse brains was prepared according to the manufacturer's protocol (FD Rapid GolgiStain kit, FD Neurotechnologies) and subsequently cut into 170 μm sections using a freezing/sliding microtome. Sections containing the hippocampus were mounted on 0.1% gelatin-coated (Sigma-Aldrich) glass slides, dried, and stored at room temperature until 0.175 μm serial-section analysis using an AxioImager wide-field microscope (63× objective, Zeiss). Tissue sections were digitally reconstructed and tertiary dentate gyrus granule cell dendrites were identified and manually traced in Neurolucida (MBF Bioscience). Dendritic spines were manually identified, counted, and

quantified as number of spines per micrometer dendrite length ($n = 4$ animals/genotype, nine dendrites/animal). The experimenter was blind to animal genotypes until after all data were analyzed. Statistical significance was determined with GraphPad Prism 5 using unpaired, two-tailed *t* test.

Immunoelectron microscopy. Cryo-immunogold electron microscopy experiments were performed based on the Tokuyasu technique (Tokuyasu, 1980). Briefly, mice were perfused with 3% formaldehyde followed by immersion of the brains in the same fixative with 0.025% glutaraldehyde for 4 h. Five-hundred micrometer-thick vibratome frontal sections were immersed in 2.3 M sucrose in phosphate buffer and 1 mm dentate gyrus areas were made with a scalpel. Samples were mounted on specimen holders and immersed in liquid nitrogen. Cryosections (90 nm) were obtained with a cryo-ultramicrotome Leica EM FC6 and collected on carbon-coated Formvar films on nickel grids. Immunogold labeling was performed by incubation with rabbit anti-C1q monoclonal antibody and anti-synaptophysin antibody for 1 h followed by washes in PBS and incubation with secondary antibodies conjugated to 12 and 6 nm gold particles, respectively, for 1 h. After washes with PBS, grids were contrasted with 0.3% uranyl acetate in methylcellulose for 5 min and examined in an electron microscope Tecnai G2 Spirit (FEI).

Hippocampal physiology. Hippocampal slices were prepared by standard methods (Madison and Edson, 2001). Briefly, hippocampi were dissected from the brains of mice, sliced in a transverse orientation using a manual razor blade tissue slicer (Stoelting), placed onto filter paper moistened with artificial CSF consisting of the following in mM: 119 NaCl, 2.5 KCl, 1.3 $MgSO_4$ 2.5 $CaCl_2$, 1 Na_2HPO_4, 26.2 $NaHCO_3$, and 11 glucose, in an atmosphere saturated with 95% O_2/5% CO_2 (carbogen). Two hours after dissection, one slice was removed to the recording chamber where it was submerged under continuously flowing artificial CSF, containing 10 μM picrotoxin and saturated with carbogen. A bipolar metal concentric stimulating electrode (Frederick Haer) was placed in the inner leaf of the dentate gyrus on the end farthest from hippocampal area CA3. The electrode spanned approximately one-half the width of the molecular layer, and was placed approximately halfway between the granule cell layer and the hippocampal fissure. Stimuli of varying strength and 100 μs duration were delivered from an AMPI Instruments constant-current stimulus isolation unit, to the molecular layer through this electrode. Resulting dendritic excitatory postsynaptic field potentials (fEPSPs) were recorded with a glass micropipette filled with 2 M NaCl placed also in the molecular layer of the dentate gyrus closer to CA3, and also halfway between the granule cell layer and the hippocampal fissure. fEPSPs were recorded using an Axoclamp 2A in bridge mode, amplified with a Brownlee Precision model 200 amplifier, and digitized at 10 kHz using a National Instruments analog-to-digital converter. The rising slope of each individual fEPSP was analyzed using a program specifically written for this purpose by Eric Schaible and Paul Pavlidis (Stanford University, Stanford, CA) in the Labview programming environment (National Instruments). For input/output (I/O) experiments, the stimulus was adjusted by increments between 0.01 and 0.7 mA. For the analysis of the relationship between the presynaptic compound action potential (fiber volley) and the fEPSP in the molecular layer (ML), the fiber volleys were aligned by binning them into 19 groups according to amplitude. An ANOVA was then run across these 19 fiber volley levels to determine a statistical significant change in the level of fEPSP responses between wild-type and C1q-deficient littermate animals. For paired-pulse facilitation experiments, two stimuli were delivered, and the interpulse interval was adjusted by increments from 10 to 1000 ms. For LTP experiments, test stimuli were delivered at a rate of 1/15 s, and an amplitude adjusted to give a response of ~2/3 maximum, for at least 30 min before delivery of tetanic stimulation. The tetanus consisted of 1 s duration trains of 100 Hz stimuli delivered at test intensity, four times, 15 s apart. Following the tetanus, the stimulus frequency was returned to 1/15 s for 70 min. For paired-pulse facilitation analysis, raw fEPSP slope measurements were averaged across experiments. For LTP experiments, data points were collected in 15 s intervals and four subsequent data points were averaged for subsequent data analysis to obtain the 1 min averages presented. Each individual experiment was then normalized against its own baseline. These normalized 1/min time points were then averaged across experiments. The experimenter was blind to the genotype of the animal until after the individual experiments were analyzed. For LTP and I/O experiments, statistical significance was determined with a two-way repeated-measure ANOVA. Statistical significance of paired-pulse facilitation data were determined with GraphPad Prism 5 using paired, two-tailed *t* test.

Mouse behavior. For every experiment/age-group presented, two individual cohorts of male mice were analyzed, each consisting of 10–18 C1q-deficient mice and 10–18 wild-type litter- and cage-mates; mouse behavior modified from Faizi et al. (2012). The genotypes of all animals were determined by PCR before and after experiments. Because of technical reasons, we were not able to analyze 3- and 17-month-old C1q cohorts in parallel. To optimize our experiments to detect aging-dependent defects in C1q wild-type mice, 10- to 12-week-old male strain-matched mice (C57BL/6, Charles River Laboratories) were used as aging-controls and a positive control in every task. All animals were group-housed after weaning until behavioral assessment was performed (up to five mice per cage, mixed genotypes per cage). Animals were housed in a 12 h dark/light cycle (lights on at 8:00 P.M.), temperature- and humidity-controlled environment with unlimited access to water and food. All tests were conducted in the dark cycle. Experimenters were blind to the genotype of the mice throughout testing. All animals tested were handled by the experimenter for three d before all the behavioral tests. In all experiments, animals were habituated to the testing room 1 h before the tests. All experiments were in accordance with protocols approved by the Institutional Animal Care and Use Committee of Stanford University and were performed based on the National Institutes of Health *Guide for the Care and Use of Laboratory Animals*. All actions were considered for reducing discomfort of animals during all experiments.

Open-field activity. The open-field test was used to assess locomotor activity and exploration habits in a relatively large novel environment. Assessment took place in a square arena (76×76 cm^2) with opaque white walls, surrounded with privacy blinds to eliminate external room cues. Mice were placed in the corner of the open-field arena and allowed to freely move for 10 min while being tracked by Ethovision (Noldus Information Technology) automated tracking system. Before each trial, the surface of the arena was cleaned with 1% Virkon. For analysis, the arena was divided into a central (53.5×53.5 cm^2) and a peripheral zone (11.25 cm wide). Distance moved, velocity, and time spent in each predefined zone was recorded.

Spontaneous alternation in the Y-maze. The Y-maze was used to assess spontaneous alternation behavior. This test is based on the innate preference of rodents to explore a new environment (Gerlai, 1998; Lalonde, 2002). We compared each group of mice to chance levels which is believed to be a sensitive method of assessing working memory function (Bertholet and Crusio, 1991; Hooper et al., 1996; Jacquelin et al., 2012). A mouse that shows a percentage of alternation above chance level is believed to have good working memory. The Y-maze was made of solid white plastic and consisted of two symmetrical arms and one longer arm at 120° angles (longer arm, 20.7 cm length × 12.7 cm height × 7.62 cm width; equal arms, 15.24 cm length × 12.7 cm height × 7.62 cm width). At the beginning of trials, mice were placed in the center of the maze and allowed to freely explore the three arms for 5 min. Arm entry was defined as having all four limbs inside an arm. The maze was cleaned with 1% Virkon between animals and before the first animal to eliminate traces of odor. The number of arm entries and the number of triads were recorded to calculate the alternation percentage, which was calculated by dividing the number of triads by the number of possible alternations multiplied by 100. A triad was defined as a set of consecutive arm entries (Drew et al., 1973; Hughes, 2004).

Morris water maze. The Morris water maze (MWM) was originally designed to test spatial reference memory in rats by observing and recording escape latency, distance moved, and velocity during the search of a hidden escape platform in a large pool (Morris, 1984). For our test, we used a large water tank (178 cm in diameter) filled with water at a temperature of 22.0 ± 1.5°C with a circular platform (17 cm in diameter) placed ~1 cm below the water surface and ~50 cm away from the wall. Nontoxic tempera paints (Elmers) were used to make the water opaque. The water tank was completely surrounded by privacy blinds with at least

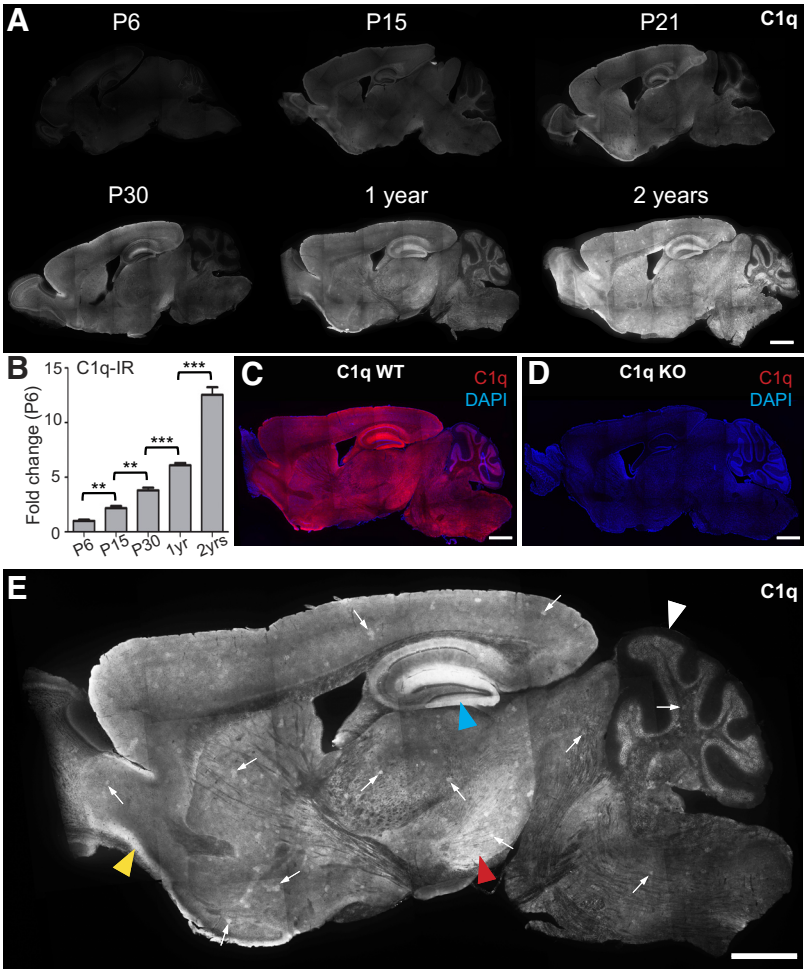

Figure 1. C1q immunoreactivity dramatically increases with aging in the murine brain. ***A***, Time course immunohistochemistry of perfused mouse brain slices with our new rabbit anti-mouse C1q monoclonal antibody revealed that C1q immunoreactivity dramatically increased with age throughout the brain. ***B***, Quantification of C1q immunoreactivity in brain slices from early postnatal to old aged mice confirmed that C1q immunoreactivity dramatically increases with aging in the murine brain. C1q signals, normalized to P6 levels ($n = 3$ brains per age; statistical significance: P15 vs P6: $p = 0.019$; P30 vs P15: $p = 0.0013$; 12 months vs P30: $p < 0.0001$; 24 vs 12 months: $p < 0.0001$). ***C***, ***D***, All C1q signals in the wild-type adult brain (***C***) were specific (images from sections of 1-year-old brains); no signals were detected in C1q-deficient littermate control tissue (***D***). ***E***, C1q-specific signals in the adult and aged brain (representative image of a brain slice from a perfused 2-year-old mouse shown) were detected throughout the brain neuropil, except in the molecular layer of the Cerebellum (white arrowhead). C1q-positive signals were particularly strong in the hippocampus (blue arrowhead), the piriform cortex (yellow arrowhead), and the substantia nigra (red arrowhead). In addition, locally increased C1q-immunoreactivity was detected in patches (C1q-positive patches) in many regions of the mouse brain neuropil (arrows; for more detail see Fig. 3). Scale bars: ***A***, ***C***, ***D***, ***E***, 1 mm; $^{**}p < 0.01$, $^{***}p < 0.001$. Values and error bars represent mean ± SEM.

four visual cues attached to the blinds. Four different shapes including a star shape, circle, rectangle, and diamond each with ~6 square feet in surface area were used as visual cues. The visual cues were located ~150 cm from the center of the tank. Testing was performed under dim white light (40 Lux at the water surface). The water tank arena was monitored by an overhead video system that allowed Ethovision to track the mice. During hidden platform training, a platform was positioned in one quadrant of the tank. Mice were released from pseudo randomized drop locations and given 60 s to find the platform. The distance to the platform was generally the same within a day. The trial either ended when the mice rested on the platform for 10 s or until the trial duration expired. If mice failed to find the submerged hidden platform during that time, they were guided to it. Mice underwent four trials of training each day (30 min intertrial intervals) for seven consecutive days. On completion of the hidden platform training, the platform was removed and a 60 s probe trial was conducted. Successful learning of MWM was determined by the gradual decrease in escape latency and discriminative quadrant exploration during the probe trial. The total amount of time spent looking for the platform per day (maximum of 240 s: four trials × 60 s each) was used for analysis. After the probe trial, mice were given 3 d of reversal learning during which the platform was positioned in a different quadrant. Following reversal training, visible platform training was performed to ensure that no gross sensorimotor or visual deficits are present. During the visible platform training, the platform was marked with a black-and-white Ping-Pong ball attached to a 10 cm wooden stick. No mice were excluded based on our standard exclusion criteria in this task: excessive thigmotaxis, obvious visual impairment, excessive corkscrew swimming pattern, and obvious sensorimotor dysfunction. The water was frequently changed and the tank disinfected.

Statistical analysis of behavior data. All data are presented as mean ± SEM and $p \leq 0.05$ was considered statistically significant. Statistical measurements were performed with GraphPad Prism 5. Percentage of alternation in the Y-maze was analyzed using a one-sample *t* test versus chance level (50% of alternation). Repeated measures two-way ANOVA was used for evaluation of the parameters in open field, water maze and fear conditioning. The Bonferroni test was used for *post hoc* analysis. Paired Student's *t* test was used in the novel object recognition test to compared the time spend exploring the new versus the familiar object. In all statistical analysis, the normal distribution of the data were tested using the Kolmogorov–Smirnov normality test.

Results

C1q protein increases dramatically in the aging brain

To determine the amount and localization of C1q protein at different maturation stages of the murine brain, we first generated a rabbit monoclonal antibody to mouse C1q that enabled high affinity detection of and absolute specificity for C1q in immunohistochemistry (IHC) applications. Using this antibody, we found that C1q immunoreactivity was low during the first postnatal week, but then gradually increased with maturation and aging throughout the neuropil of the perfused mouse brain (Fig. 1*A*). When normalizing to whole brain IHC signal levels from individual postnatal day (P)6 brain slices (Fig. 1*B*), we found that C1q immunoreactivity increased till the end of the second postnatal week by approximately twofold (P15: 2.17 ± 0.19-fold, $p = 0.019$; P15 vs P6), to approximately fourfold at 1 month (P30: 3.80 ± 0.24-fold, $p = 0.0013$; P30 vs P15), to approximately sixfold at 1 year (6.10 ± 0.21-fold, $p < 0.0001$; 12 months vs P30) and reached an ~12.5-fold increase at 2 years of age (12.54 ± 0.71-fold, $p < 0.0001$; 24 vs 12 months; $n = 3$ brains per age). All C1q immunoreactivity was absolute specific for C1q as no staining was detectable in brain sections from C1q-deficient mice using various conditions and immunohistochemistry techniques (see Figs. 1*C,D*, 3*C,D*, 5*I,J*, 6*D,E*). In addition, the age-dependent appearance and distribution of C1q immuno-

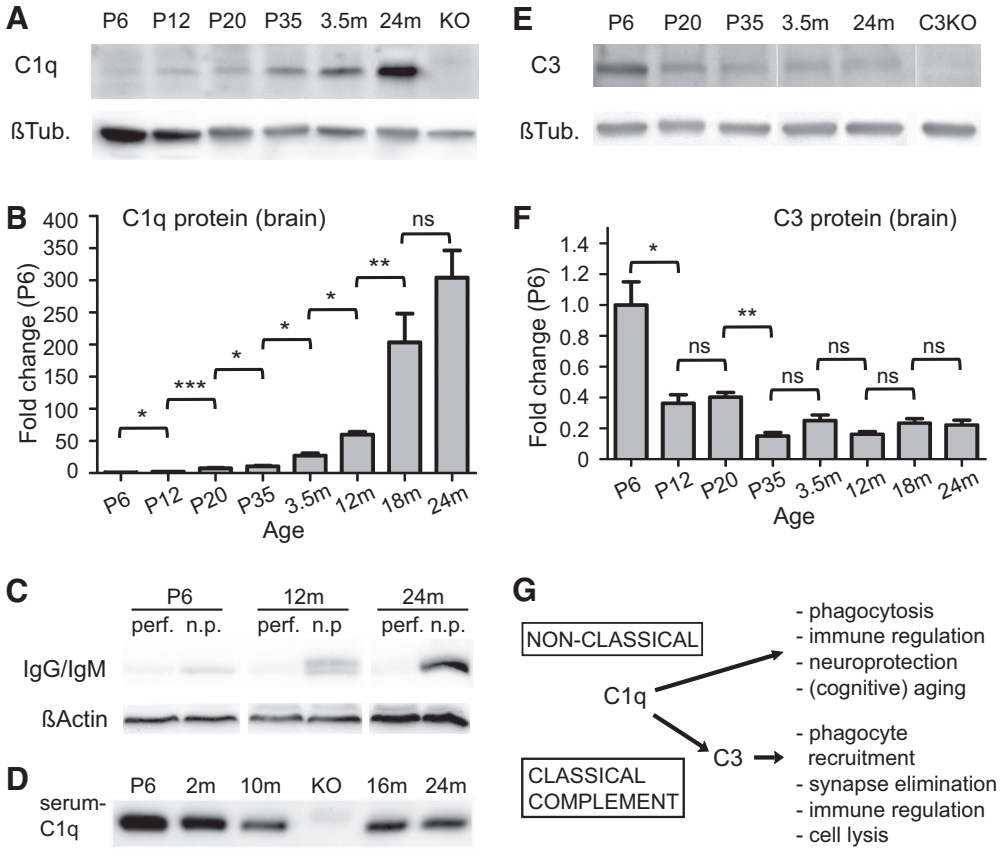

Figure 2. C1q protein levels dramatically increase with aging in the murine brain. ***A***, Western blot analysis of perfused, whole-brain homogenates using a commercially available anti-mouse C1q polyclonal antibody confirmed that C1q protein dramatically increased with aging in the murine brain, when compared with β-tubulin (βTub) loading controls. C1q signals detected were specific (KO, C1q-deficient brain homogenate). ***B***, Quantification of Western blot signals, normalized to β-Tub loading controls, confirmed that C1q protein dramatically increased with age (C1q levels, normalized to P6 levels, $n = 3$ animals/age; statistical significance: P12 vs P6: $p = 0.019$; P20 vs P12: $p = 0.0005$; P35 vs P20: $p = 0.019$; 3.5 months vs P35: $p = 0.043$; 12 vs 3.5 months: $p = 0.012$; 18 vs 12 months: $p = 0.0017$; 24 vs 18 months: $p = 0.104$). ***C***, Serum components IgG and IgM were only detected in nonperfused (n.p.) but not in perfused (perf) brains at all ages. ***D***, C1q immunoreactivity did not increase with age in mouse serum (equal protein concentration loaded). ***E***, Western blot analysis of perfused, whole-brain homogenates revealed that C3 immunoreactivity did not increase with age, compared with the β-Tub loading controls. C3 signals were specific (C3KO, C3-deficient brain homogenate). ***F***, Quantification of Western blot-derived C3 signals, normalized to β-Tub loading controls, confirmed that C3 protein decreased from early postnatal ages to approximately 1 month of age and after (C3 levels, normalized to P6 levels, $n = 3$ animals/age; statistical significance: P12 vs P6: $p = 0.029$; P20 vs P12: $p = 0.434$; P35 vs P20: $p = 0.003$; 3.5 months vs P35: $p = 0.07$; 12 vs 3.5 months: $p = 0.18$; 18 vs 12 months: $p = 0.50$; 24 vs 18 months: $p = 0.88$.). ***G***, Schematic overview of the known classical complement (C3)-dependent and nonclassical (C3-independent) functions of C1q (Ricklin et al., 2010; Veerhuis et al., 2011; Nayak et al., 2012; Stephan et al., 2012). m, Month; ns, not significant; $^*p < 0.05$, $^{**}p < 0.01$, $^{***}p < 0.001$. Values and error bars represent mean ± SEM.

reactivity was independent of mouse gender and strain (data not shown).

Particularly strong C1q-immunoreactivity in the adult and aging mouse brain was detected in the piriform cortex (Fig. 1*E*, yellow arrowhead), the substantia nigra (Fig. 1*E*, red arrowhead) and within the hippocampus (Fig. 1*E*, blue arrowhead). In addition, in the adult and aged mouse brain, high levels of C1q immunoreactivity were also detected in patches that were found scattered throughout the brain neuropil, each enclosing only a few neurons (Fig. 1*E*, arrows). We termed these previously unrecognized structures "C1q-positive patches" (see Fig. 3 and section below). Interestingly, the only neuropil-region in the mouse CNS that did not show an increase of C1q-levels with aging was the cerebellar molecular layer (Fig. 1*E*, white arrowhead).

To determine the degree of increase of C1q protein levels in the aging brain with higher sensitivity, we next performed quantitative Western blotting using a commercially available polyclonal antibody against C1q (Fig. 2*A*). Compared with P6, we found that C1q levels indeed gradually increased with age in whole brain-homogenates to ~27-fold in 3-month-old mice, then further doubled by 12 months of age and reaching maximum levels of ~300-fold at 18–24 months of age [Fig. 2*B*; fold-increase/age, normalized to P6 levels: P12: 3 ± 0.24, $p = 0.019$ (P12 vs P6); P20: 8 ± 0.60, $p = 0.0005$ (P20 vs P12); P35: 12 ± 1.04, $p = 0.019$ (P35 vs P20); 3.5 months: 27 ± 3.73, $p = 0.043$ (3.5 months vs P35); 12 months: 59 ± 3.10, $p = 0.012$ (12 vs 3.5 months); 18 months: 204 ± 12.29, $p = 0.0017$ (18 vs 12 months); 24 months: 301 ± 33.32, $p = 0.104$ (24 vs 18 months), $n = 3$ animals/age]. Serum is a major location of C1q in the periphery, however the age-dependent increase of C1q was not an artifact of serum contamination as serum proteins were only detected in nonperfused brains and not in the perfused tissue used for all C1q analyses (Fig. 2*C*). Furthermore, C1q IHC was not associated with blood vessels in the CNS and we did not detect an age-dependent increase of serum C1q levels by standard Western blotting analysis (Fig. 2*D*). C3 is an effector of the classical complement cascade and present in high amounts in the juvenile mouse brain, where it is required for part of developmental synapse elimination (Stevens et al., 2007). In contrast to the large increase in C1q levels observed with aging, we found that the levels of C3 protein in the CNS significantly decreased with age and were present at only low levels just above the detection limit

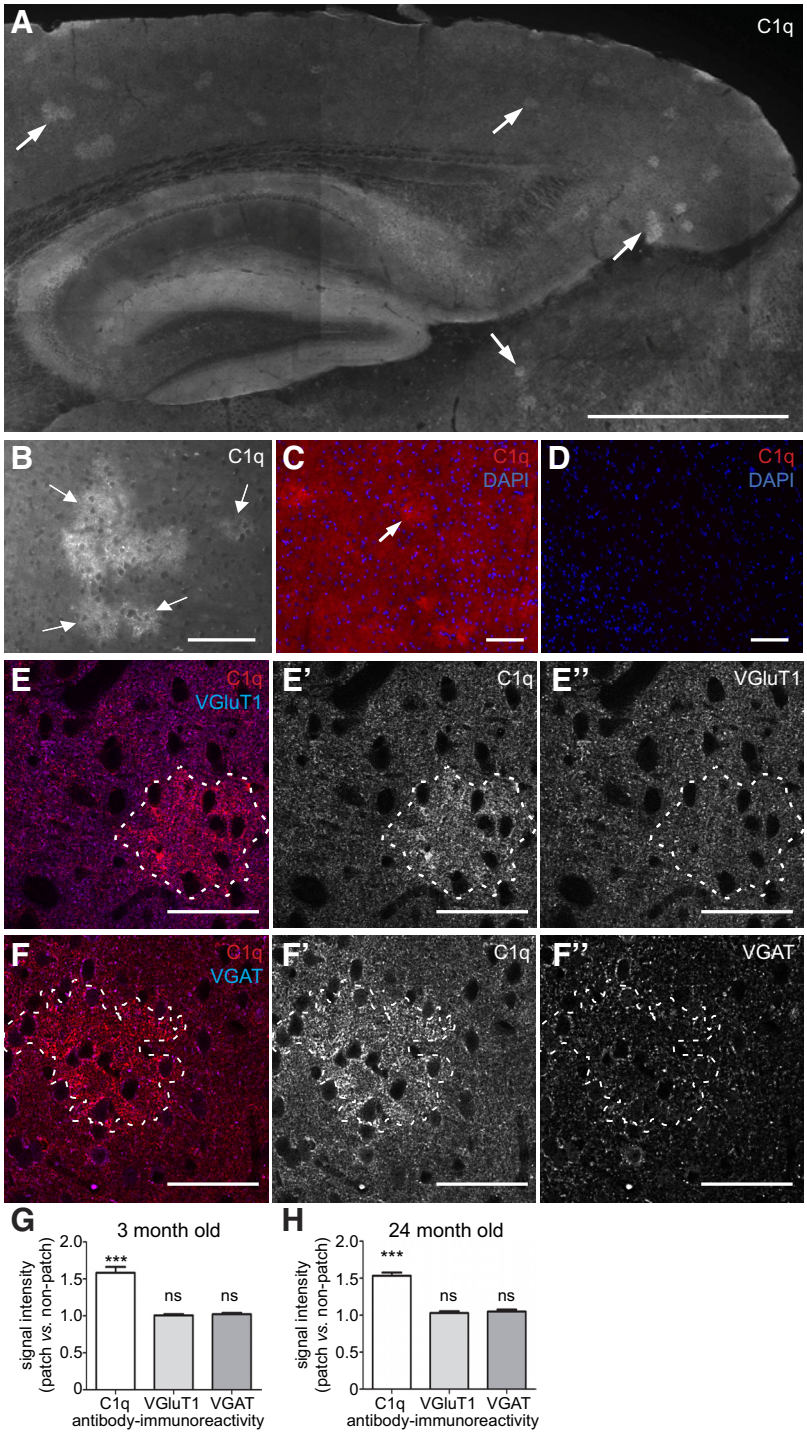

Figure 3. Characterization of C1q-positive patches in the mouse brain. ***A***, Representative immunohistochemistry image of an adult mouse brain slice (perfused animal), stained with our new rabbit anti-mouse C1q monoclonal antibody. C1q-positive patches appeared throughout the brain (arrows; 12 months old). ***B***, Higher-magnification images depicting the variability in appearance of these C1q-positive patches (arrows). ***C***, ***D***, C1q signals including the C1q-positive patches were exclusively detected in wild-type tissue (***C***) and, thus, specific; no signals were detected in C1q-deficient littermate control tissue (***D***; 9 months old). ***E***, ***F***, Confocal microscopy coexpression analyses for C1q and the excitatory synaptic protein VGluT1 (***E***) or the inhibitory synaptic protein VGAT (***F***) revealed that the overall synaptic pattern or density was not altered in C1q-positive patches. Whereas C1q-immunoreactivity was increased in patch areas (hatched lines) over areas outside the patches, both VGlut1 and VGAT immunoreactivity appeared unchanged inside or outside the C1q-positive patches. ***G***, ***H***, Quantification of antibody-immunoreactivity confirmed that C1q-immunoreactivity was increased in C1q-positive patches, compared with outside-patch signal intensities (3-month-old, $p < 0.0001$; 24-month-old, $p < 0.0001$; $n = 3$ animals per age). In contrast to C1q, VGluT1 and VGAT immunoreactivities were similar inside or outside C1q-positive patch areas at both ages analyzed [3-month-old: VGluT1 ($p = 0.68$), VGAT ($p = 0.25$); 24-month-old: VGluT1 ($p = 0.25$), VGAT ($p = 0.07$); $n = 3$ animals per age]. ***$p < 0.001$. Values and error bars represent mean ± SEM. Scale bars: ***A***, 1 mm; ***B–D***, 100 μm; ***E***, ***F***, 50 μm.

from early adulthood on into old age [Fig. 2*E,F*; fold-increase/age, normalized to P6 levels: P12: 0.43 ± 0.07, $p = 0.029$ (P12 vs P6); P20: 0.41 ± 0.05, $p = 0.434$ (P20 vs P12); P35: 0.12 ± 0.01, $p = 0.003$ (P35 vs P20); 3.5 months: 0.26 ± 0.07, $p = 0.07$ (3.5 months vs P35); 12 months: 0.17 ± 0.01, $p = 0.18$ (12 vs 3.5 months); 18 months: 0.23 ± 0.02, $p = 0.50$ (18 vs 12 months); 24 months: 0.22 ± 0.03, $p = 0.88$ (24 vs 18 months); $n = 3$ animals/age]. Together these findings demonstrate that C1q, but not C3, protein levels increase profoundly in the CNS, throughout the brain neuropil during normal brain maturation and aging, potentially suggesting complement-independent functions for C1q during normal brain aging (Fig. 2*G*).

Identification of novel C1q-positive structures

Starting in adulthood, as mentioned above (Fig. 1*E*), high levels of C1q immunoreactivity were also detected in a previously unrecognized type of structure, which consisted of patches of ~20–150 μm diameter that were found scattered throughout the brain neuropil, each enclosing only a few neurons (Figs. 1*E*, 3*A–F*). These C1q-positive patches were highly variable in size and distribution, and were mainly detected in the cortex, thalamus, midbrain, and striatum but were much less frequent in the cerebellum and hippocampus (Figs. 1*E*, 3*A*). Quantification of C1q-immunoreactivity in brain sections from adult and aged mice revealed that C1q signals were increased in C1q-positive patches by 1.58 ± 0.07-fold (3-month-old; $p < 0.0001$) and 1.53 ± 0.04-fold (24 months old; $p < 0.0001$), compared with outside-patch signal intensities, and thus confirmed that their relative intensity did not increase with aging after their appearance in the adult mouse brain. In contrast to C1q, the degree of both excitatory and inhibitory synaptic protein densities (VGluT1, Fig. 3*E,G,H*; VGAT, Fig. 3*F–H*, respectively) in these patches was similar to that of the nearby neuropil which argues against C1q-positive patches being regions of increased synapse loss [Fig. 3*G,H*; immunoreactivity inside patch vs outside patch region; VGluT1: 1.01 ± 0.02-fold (3-month-old; $p = 0.68$) and 1.03 ± 0.02-fold (24 months old; $p = 0.25$); VGAT: 1.02 ± 0.02-fold (3-month-old; $p = 0.25$) and 1.05 ± 0.03-fold (24 months old; $p = 0.07$); $n = 3$ animals/age]. Furthermore, these characteristics, along with their differing appearance, suggest that C1q

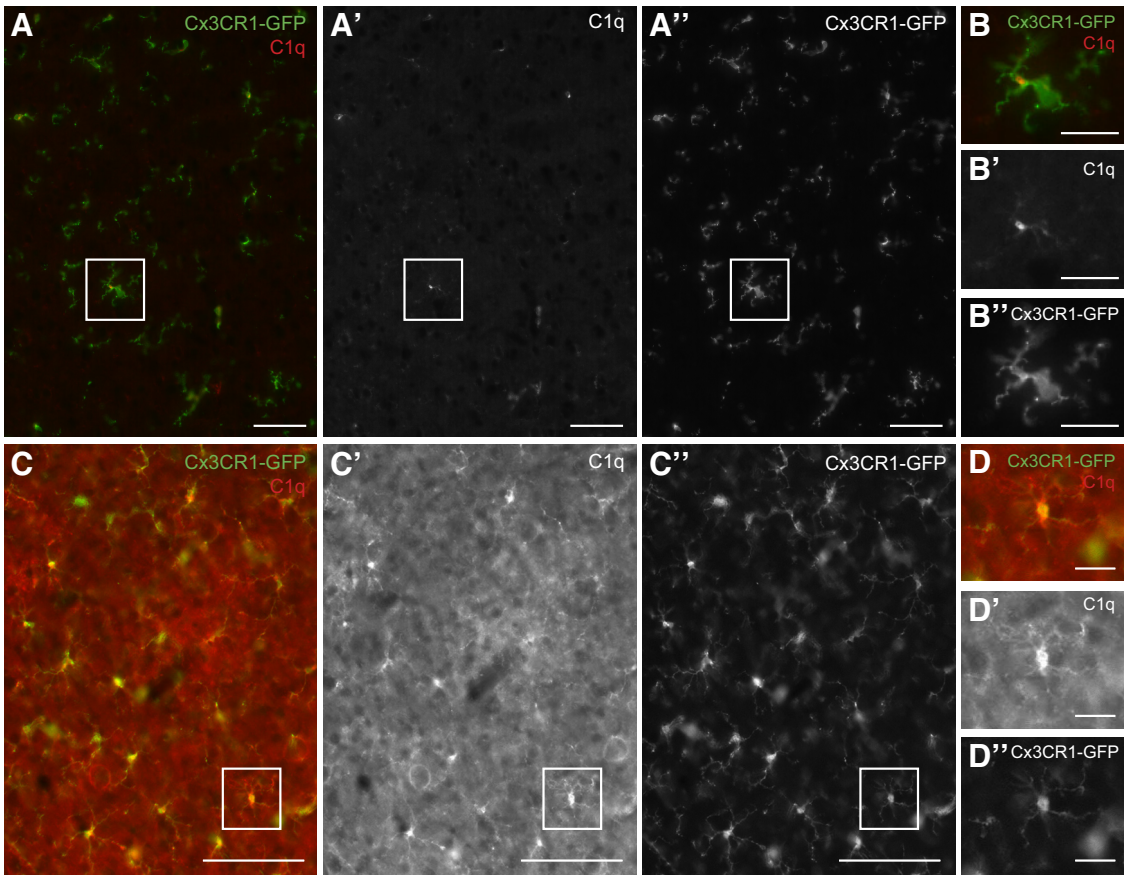

Figure 4. C1q immunoreactivity was detected at all developmental stages in microglia throughout the CNS. ***A***, ***B***, Colocalization immunohistochemistry analysis (our new rabbit anti-mouse C1q monoclonal antibody) confirmed that C1q immunoreactivity in the perfused P6 mouse brain was virtually exclusively detected in microglia, visualized by GFP immunoreactivity in slices from *Cx3CR1-GFP* $^{+/-}$ mice (image representative for all brain regions; image location: midbrain; boxed area in ***A*** is shown as magnified image in ***B***). ***C***, ***D***, In contrast, C1q immunoreactivity in the perfused 9-month-old mouse brain was substantially increased in all microglia and additionally detected at high levels in the neuropil throughout the brain (Cx3CR1-GFP signals; image representative for all brain regions; image location: midbrain; boxed area in ***C***, is shown as magnified image in ***D***. Please note that ***A***, ***B*** were taken with increased image exposure times compared with ***C***, ***D***). Scale bars: ***A***, 50 μm; ***B***, ***D***, 20 μm; ***C***, 100 μm.

patches are not amyloid plaques but represent a novel structure of unknown significance and function.

C1q immunoreactivity in microglia and a subset of inhibitory neurons

We next investigated the exact cellular localization of C1q immunoreactivity in the adult brain. We detected C1q-immunoreactivity at all developmental stages inside most or all microglia (Figs. 4, 5*C*,*D*; see Fig. 6*A*), correlating with their well described expression of C1q mRNA (Schmid et al., 2009). Although C1q immunoreactivity was virtually exclusively detected in microglia throughout the early postnatal brain (Fig. 4*A*,*B*), in the adult and aged mouse brain it was detected at increased levels in all microglia as well as throughout the neuropil (Figs. 4*C*,*D*, 5*C*,*D*). In addition, from early adulthood on, strong C1q immunoreactivity was present in a distinct population of larger cells, exclusively detected in the hippocampus, thalamus, midbrain and striatum (Fig. 5*A*,*B*, as a representative overview). These cells represented a subset of neurons as confirmed by confocal microscopy colocalization analysis with the neuronal nuclear marker NeuN (Fig. 5*E*). Furthermore, all C1q-positive neurons were inhibitory neurons as identified by colocalization with GABA immunoreactivity (Fig. 5*F*,*G*, hippocampus shown as representative example). Although 100 percent of all C1q-positive neurons in the hippocampus were GABAergic, only 40.3 ± 1.8 percent (3-month-old) and 37.3 ± 2.3 per cent (24 months old) of GABAergic neurons were C1q-positive (Fig. 5*H*; $n = 3$ animals/age), confirming that they represent a subset of inhibitory neurons in the adult mouse brain. Thus, both microglial cells and a subset of inhibitory neurons exhibit strong C1q immunoreactivity; however, after early adulthood the degree of this immunoreactivity did not increase with aging.

C1q immunoreactivity accumulates with aging in close proximity to synapses

With aging, C1q immunoreactivity was particularly strong in distinct hippocampal synaptic layers, in particular the dentate gyrus ML and the stratum lacunosum moleculare of both the mouse (Fig. 6*A*,*B*) and the human hippocampus (Fig. 6*L*,*M*). When normalizing to C1q IHC signal levels in the mouse ML of P6 brain slices, we found that C1q immunoreactivity increased dramatically in the dentate gyrus molecular layer of the aging mouse to ~20-fold at 2 years of age [Fig. 6*C*; normalized to P6 levels: P30: 8.60 ± 0.54-fold increase, $p < 0.001$ (P30 vs P6); 24 months: 20.29 ± 0.52-fold increase, $p < 0.0001$ (22 months vs P30); $n = 3$ brains per age]. A similar aging-dependent increase of C1q-immunoreactivity was detected in the ML of aged human donors to approximately eightfold of infant levels (Fig. 6*N*; normalized to 1-month-old donor levels, 2 months old: 1.05 ± 0.04, $p < 0.79$ (2 vs 1 month); 75

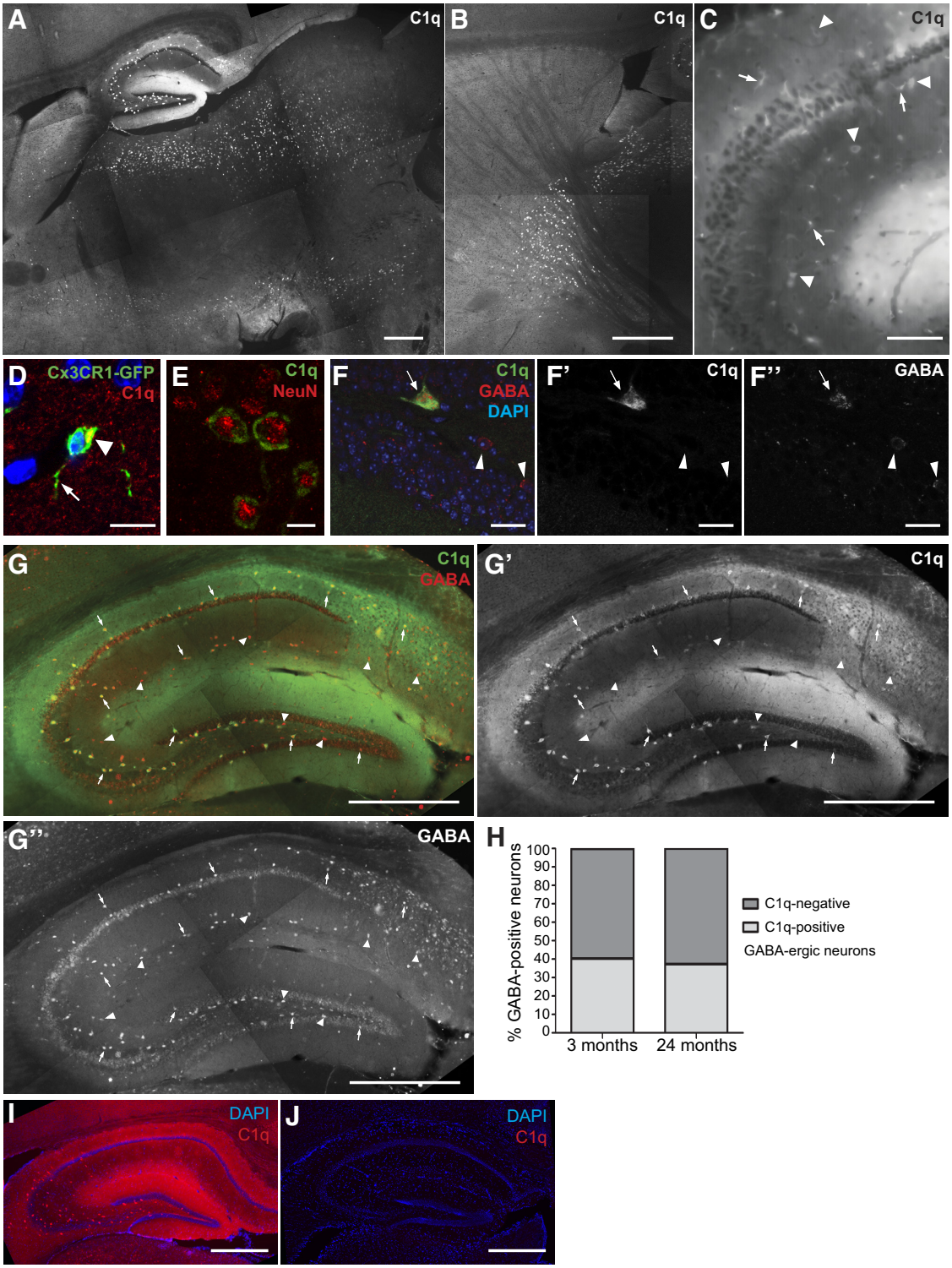

Figure 5. C1q immunoreactivity in inhibitory neurons. ***A***, ***B***, In lightly fixed tissue, our new rabbit anti-mouse C1q monoclonal antibody enabled the additional detection of C1q signals in larger cell bodies (neurons, ***E–G***), in distinct areas of the brain. These C1q-positive neurons were detected from ~1 month of age on and aging-independent thereafter (6-month-old shown). C1q-positive neurons were detected in the hippocampus, thalamus, striatum, and midbrain. The exact distribution of C1q-positive neurons visible varied slightly dependent on the location of the slices within the brain. ***A***, Detection of C1q-positive neurons in the hippocampus, thalamus, and midbrain (substantia nigra area). ***B***, Detection of C1q-positive neurons in the thalamus and striatum (mainly globus pallidus). ***C***, In the adult murine hippocampus, C1q immunoreactivity was detected in the neuropil and in both neurons (arrowhead) and microglia (arrow). ***D***, Confocal microscopy colocalization with GFP-immunoreactivity (*Cx3CR1-GFP* $^{+/-}$ mice) confirmed that C1q was detected in microglia cell bodies (arrowhead) and processes (arrow). ***E***, Confocal microscopy colocalization with NeuN-immunoreactivity confirmed that C1q was also localized to the cytoplasm of some neurons. ***F***, Confocal microscopy colocalization with GABA-immunoreactivity confirmed that C1q was localized to inhibitory neurons (arrow) but that C1q was not detected in all GABA-positive neurons (arrowheads). ***G***, C1q-positive neurons represent a subset of inhibitory neurons. Neuronal C1q signals exclusively colocalize (arrow) with many but not all GABA-positive neurons in the murine hippocampus (arrowheads: GABA+/C1q− neurons). ***H***, Quantification of C1q-GABA-positive neurons in the murine hippocampus confirmed that C1q-positive neurons represent a subset of inhibitory neurons. At both 3 and 24 months of age all C1q-positive neurons were GABAergic ($n = 3$ animals/age). ***I***, ***J***, C1q signals, including signals in neurons, are specific in the wild-type adult hippocampus (***I***), no signals were detected in the C1q-deficient littermate control (***J***). Scale bars: ***A***, ***B***, ***G***, ***I***, ***J***, 500 μm; ***C***, 100 μm; ***D***, ***E***, 10 μm; ***F***, 20 μm.

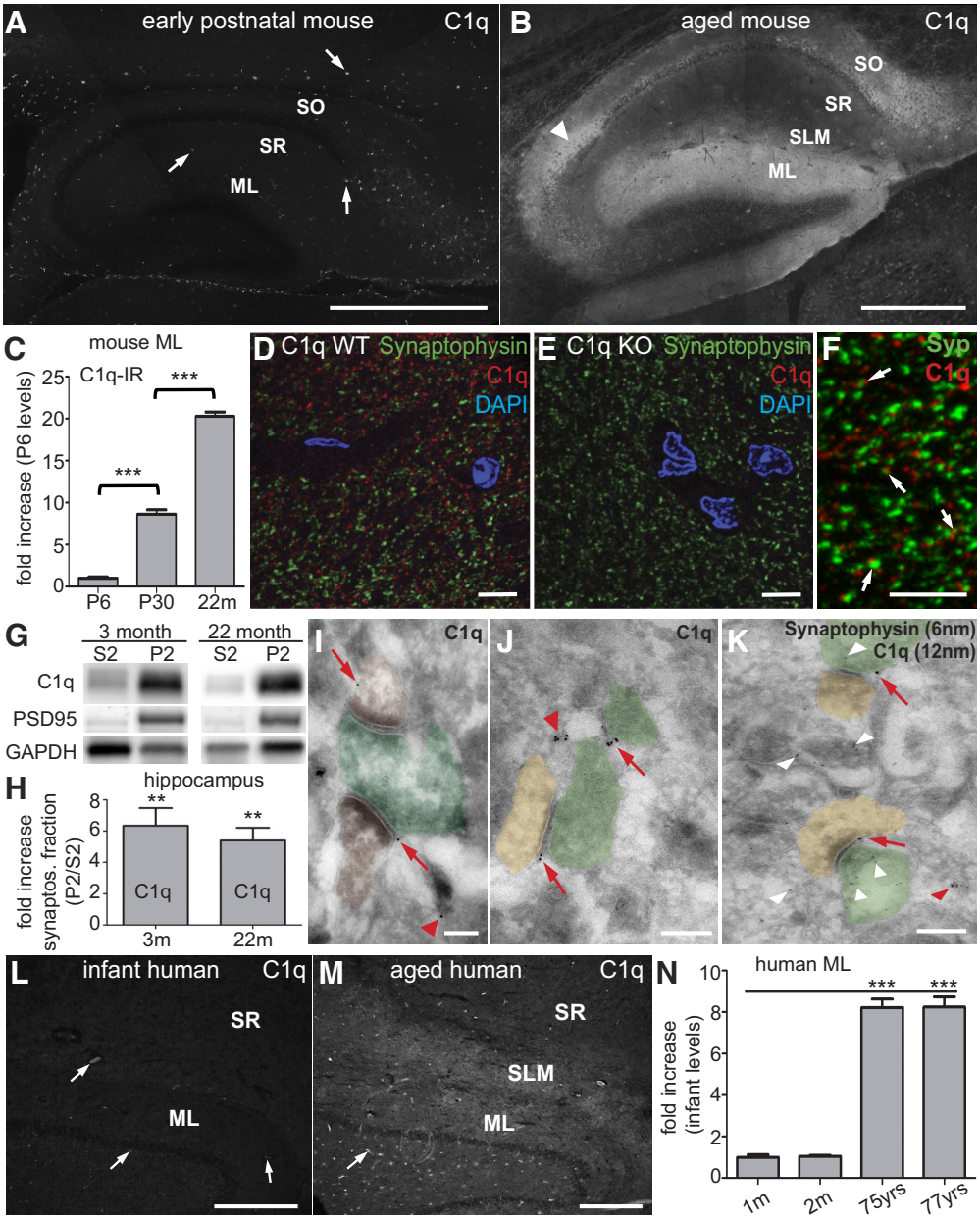

Figure 6. C1q immunoreactivity dramatically increases with age in hippocampal synaptic layers and at synapses. ***A***, ***B***, Immunohistochemistry analysis confirmed comparably low levels of C1q immunoreactivity (arrows) in the hippocampus of P6 mice (***A***) but dramatically increased levels in all synaptic layers of the 24-month-old murine hippocampus (***B***): stratum oriens (SO), stratum radiatum (SR), stratum lacunosum moleculare (SLM), dentate gyrus ML. Very strong C1q immunoreactivity was also detected in the neuropil surrounding the CA2 cell bodies (arrowhead). ***C***, Quantification of C1q immunoreactivity in the ML from early postnatal to old aged mice confirmed that C1q immunoreactivity dramatically increases with aging in the murine ML. C1q signals, normalized to P6 levels ($n = 3$ brains per age; statistical significance: P30 vs P6: $p < 0.001$; 22 months vs P30: $p < 0.0001$). ***D***, ***E***, Anti-C1q immunohistochemistry signals (rabbit anti-mouse C1q monoclonal antibody) visualized by confocal microscopy were specific. C1q immunoreactivity was only detected in the adult wild-type dentate gyrus molecular layer (***D***) but not in the corresponding tissue from C1q-deficient littermate mice (***E***). ***F***, High resolution confocal microscopy revealed that C1q immunoreactivity in the ML was detected in close proximity to synaptic terminals (synaptophysin immunoreactivity, arrows). ***G***, Subcellular fractionation of murine hippocampus homogenate revealed that C1q (detected with a polyclonal anti-C1q antibody) was enriched in the crude synaptosomal fractions (P2) from both adult and aged mice, similar to the synaptic protein PSD95, compared with the supernatant fraction (S2; representative images; GAPDH loading control). ***H***, Quantification of the hippocampal subcellular fractionation analysis confirmed that C1q was enriched in the crude synaptosomal fraction (P2) from both 3-month-old ($p = 0.0091$) and 22-month-old ($p = 0.0055$) mice ($n = 4$ animals/age), compared with the counter-fraction S2. ***I–K***, Single-section cryo-immuno electron microscopy confirmed that C1q immunoreactivity (12 nm gold particles) was detected in close proximity to the extracellular side of presynaptic- (pseudo-colored in green) or postsynaptic- (pseudo-colored in brown) elements (red arrows) and associated with unidentifiable structures (red arrowheads). This single-section image analysis did not allow clear identification of all elements visible in each section. It was therefore impossible to classify C1q immunoreactivity associated with unidentified elements as synaptic or nonsynaptic. ***K***, Dual-immunogold analysis in the dentate gyrus molecular layer of aged mice. C1q immunoreactivity (12 nm gold particles, arrows) was detected in close proximity to both presynaptic (green) and postsynaptic (brown) elements. In contrast, synaptophysin immunoreactivity (6 nm gold particles, white arrowheads) was detected inside clearly identifiable presynaptic terminals as well as associated with unidentifiable structures, likely reflecting presynaptic terminals. ***L***, ***M***, C1q immunoreactivity dramatically increased with age in synaptic layers of the human hippocampus. ***L***, C1q immunoreactivity in the human infant (2-month-old) was restricted to blood vessels (arrows), indicating serum-derived C1q in this nonperfused tissue, whereas it was particularly enriched in the SLM and ML of aged human donors (***M***; 75 years old). ***N***, Quantification of C1q immunoreactivity in the ML from available infant and old aged human donor tissue confirmed that C1q immunoreactivity dramatically increased with aging in the human ML. C1q signals, normalized to 1 month levels ($n =$ 4 slices per donor; statistical significance: 1 vs 2 months: $p < 0.79$; 1 month vs 75 years: $p < 0.0001$; 1 month vs 77 years: $p < 0.0001$). $^{**}p < 0.01$, $^{***}p < 0.001$. Values and error bars represent mean ± SEM. Scale bars: ***A***, ***B***, ***L***, ***M***, 500 μm; ***D–F***, 5 μm; ***I–K***, 200 nm.

years old: 8.22 ± 0.41, $p < 0.0001$ (75 years vs 1 month); 77 years old: 8.25 ± 0.49, $p < 0.0001$ (77 years vs 1 month); $n =$ 4 slices per donor).

As the most prominent increase in C1q immunoreactivity during aging occurred in the CNS neuropil and in particular the ML, we next investigated whether C1q was localized to ML synapses. Using confocal microscopy we found that the C1q signals were closely associated with the synaptic protein synaptophysin (Fig. 6*D–F*). In addition, performing biochemical fractionation of hippocampus homogenates from both adult and old aged mice, C1q was enriched in the crude synaptosomal fraction (P2) that is enriched in synaptic structures, when compared with the counter fraction (S2) mostly depleted of synaptic structures as indicated by PSD95 immunoreactivity [Fig. 6*G,H*; P2/S2 C1q signal quantification, 3 months of age: 6.34 ± 1.12-fold increase ($p = 0.0091$); 22 months of age: 5.42 ± 0.81-fold increase ($p = 0.0055$); $n = 4$ animals/age]. Consistent with these findings, using cryo-immuno electron microscopy, we found that C1q protein was localized to and near to the surfaces of presynaptic and postsynaptic structures (Fig. 6*I–K*) in the adult and aging brain. The single-section analysis performed did not allow 3-D reconstruction of tissue samples, and thus quantification of synaptic versus nonsynaptic C1q levels. However, anti-C1q immunoreactivity was frequently detected in close proximity to pre-or postsynaptic elements (Fig. 6*I–K*, red arrows), in addition to association with unidentifiable structures (Fig. 6*I–K*, red arrowheads). This was comparable to the signal distribution of anti-synaptophysin immunoreactivity, which was detected in clearly identifiable presynaptic terminals and associated with undefinable structures, presumably presynaptic elements (Fig. 6*K*, white arrowheads). Together, biochemical and immunohistochemistry techniques confirm that the majority of C1q protein detected in the neuropil is associated with synaptic elements in the adult and aging brain, and thus that the age-dependent increase of C1q protein in the brain mainly occurs in close proximity to synapses.

The increase of C1q-levels with CNS maturation and aging causes reorganizations of the circuitry independent of synapse elimination

The synaptic localization and dramatic increase of C1q with aging, along with its particularly prominent localization in the ML of the hippocampus, raised the question of whether the age dependent increase in C1q affected synapse number. We therefore quantified excitatory postsynaptic element numbers in the outer ML of Golgi-stained tissue. However, dendritic spine numbers were unaltered between aged C1q-deficient mice and their wild-type littermates (Fig. 7*A,B*; 18-month-old, wild-type: 2.37 ± 0.15 spines/μm; C1q-deficient littermates: 2.18 ± 0.20 spines/μm; $p = 0.47$; $n = 4$ animals/genotype), arguing against a correlation of increased C1q levels with synapse elimination in normal CNS aging.

We further examined basal synaptic transmission in the ML (Fig. 7*C*), measured as the input/output relationship between activation (amplitude of the presynaptic compound action potential, fiber volley) and the fEPSP I/O curve. Neither juvenile, adult, nor aged C1q-deficient mice displayed a significant change in this I/O curve (Fig. 7*D*; P14–P17, $p = 0.896$; $n = 6$ wild-type, $n = 6$ C1q-deficient littermates; Fig. 7*E*; 3-month-old, $p = 0.284$; $n = 10$ wild-type, $n = 12$ C1q-deficient littermates; Fig.7*F*; 17-month-old, $p = 0.494$; $n = 13$ wild-type, $n = 11$ C1q-deficient littermates), suggesting that C1q deficiency does not result in a significant change in the ratio of presynaptic axons to synapses at any age in the dentate ML. Interestingly, we found that the relationship between the applied stimulus and the fiber volley was significantly suppressed in adult and aged (Fig. 7*H,I*; $p = 0.05$, $p = 0.0486$, respectively) but not in juvenile C1q-deficient mice (Fig. 7*G*; $p = 0.86$), compared with their wild-type littermates. This indicates that either the number of presynaptic axons or their excitability is decreased in the ML of aging C1q-deficient mice. Together, these physiology results suggest that if anything, the presence of C1q enhances synapse number with aging, but certainly does not decrease it. The relationship between the applied stimulus and the resulting fEPSPs (data not shown) was not significantly different between C1q-genotypes at any age, reinforcing the idea that C1q does not reduce the overall number of synapses in the ML of the dentate gyrus. Thus, these findings identify a novel function for C1q in impacting circuit diversity with aging that is independent of classical complement-mediated synapse pruning.

To investigate whether the dramatic increase of C1q at aging synapses impacts synaptic plasticity, we analyzed activity-dependent synaptic potentiation of perforant path to dentate gyrus synapses (Fig. 7*C*) in C1q-deficient mice compared with their wild-type littermates. Interestingly, adult C1q-deficient mice showed enhancements in both post-tetanic potentiation [PTP; Fig. 8*B*; 3-month-old, PTP, wild-type: 164.6 ± 3.5; C1q-deficient: 200.8.1 ± 7.1 fEPSP (% baseline), $p = 0.008$] and subsequent potentiation when compared with their wild-type littermates [Fig. 8*B*, potentiation after PTP decay, 5–10 min after tetanus, wild-type: 119.5 ± 0.7; C1q-deficient: 144.9 ± 0.6 fEPSP (% baseline), $p = 0.049$; potentiation was significantly different for the time-span from 3 to 20 min post-tetanus, $p = 0.049$]. Potentiation also decayed faster in adult C1q-deficient mice ($p < 0.001$); however, at 1 h post-tetanus, potentiation in C1q-deficient and wild-type littermates had decayed to similar values (wild-type 110.2 ± 0.8 and C1q-deficient 116.0 ± 0.6, $p = 0.634$). In contrast, no differences between C1q-deficient and wild-type littermates were detected in juvenile mice (Fig. 8*A*, P14–P17) or aged mice (Fig. 8*C*, 17-month-old) as synaptic potentiation after tetanic stimulation, both immediately after tetanic stimulation (PTP juvenile: $p = 0.554$; PTP aged: $p = 0.671$) and later potentiation (juvenile: $p = 0.867$; aged: $p = 0.205$) were nearly identical between C1q-deficient and wild-type littermates mice. In accordance with the substantial age-dependent increase of C1q protein already in the maturing ML, this indicates that C1q exerts a negative effect on synaptic plasticity in the adult but not juvenile or old aged ML. Paired-pulse facilitation analysis did not reveal any differences between C1q-deficient mice and their wild-type littermates, suggesting that the potentiation phenotype in adult mice is not driven by altered presynaptic facilitation (data not shown). As neither juvenile C1q-deficient mice (Fig. 8*A*) nor adult C3-deficient mice (Fig. 8*D*) have increased potentiation after tetanic stimulation, the enhanced potentiation in adult C1q-deficient mice reflects a novel synaptic function of C1q, independent of complement-cascade activity. Interestingly, adult C3-deficient mice showed an inverse LTP-phenotype to adult C1q-deficient mice, as potentiation in C3-deficient mice was significantly reduced for the entire post-tetanus time-span when compared with their wild-type littermates (Fig. 8*D*, $p = 0.044$). These data suggest that C1q and C3 also have individual functions in the CNS beyond classical complement activation. Together, these findings identify novel functions for C1q and C3 by independently affecting LTP in the dentate gyrus, in particular for C1q in negatively modulating synaptic plasticity of the adult

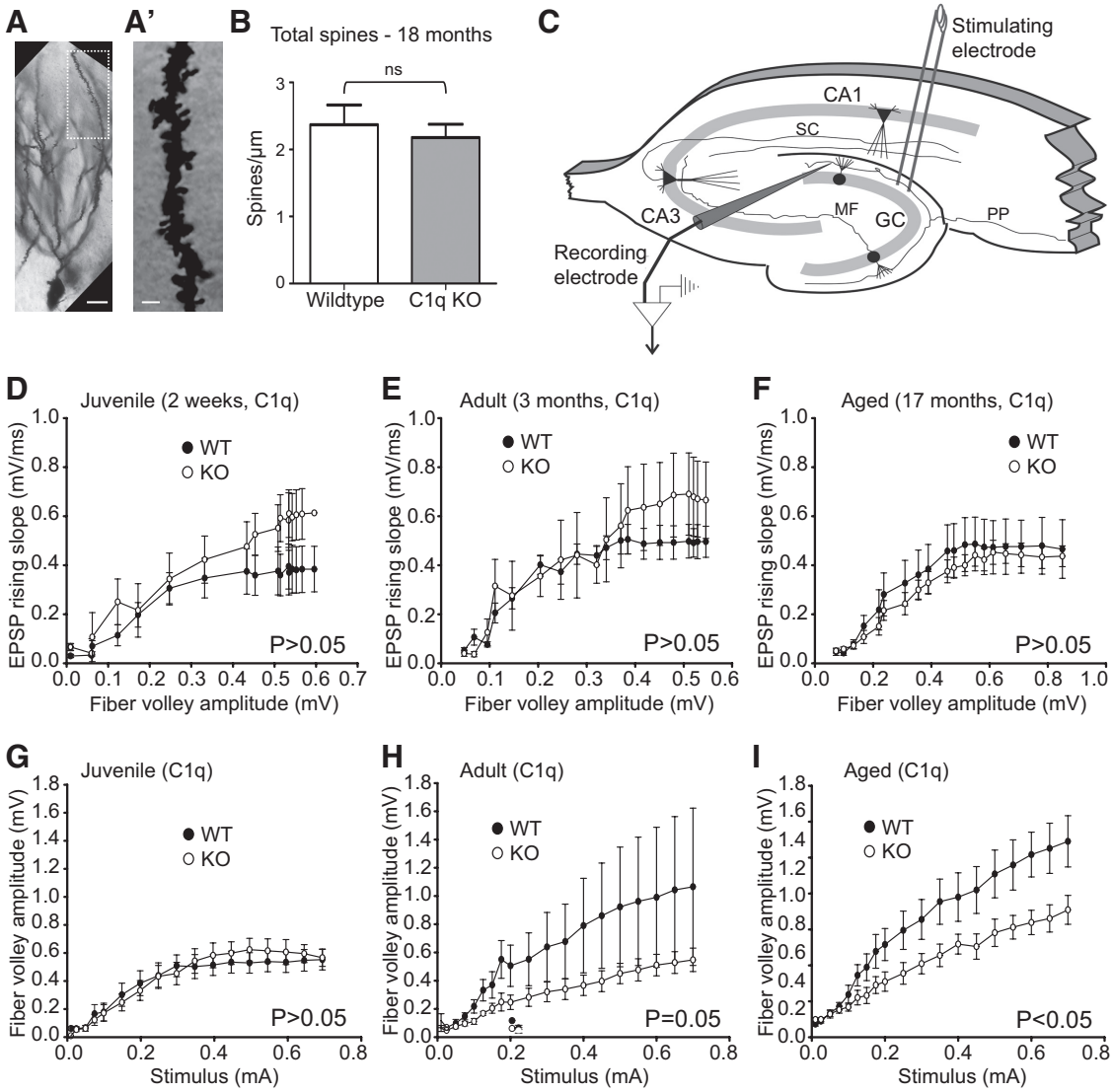

Figure 7. C1q-deficiency impacts the neuronal circuitry in the dentate gyrus of adult and aging mice. ***A***, Representative example of a Golgi-stained dentate gyrus granule cell neuron and the approximate dendritic segment (boxed area) used for the dendritic spine quantification analysis from an 18-month-old mouse. A representative higher-magnification image of a tertiary dentate gyrus granule cell dendrite segment in the outer molecular layer, used for quantification, is shown in ***A′***. ***B***, Tertiary dentate gyrus granule cell dendrites in the outer molecular layer of the dentate gyrus from 18 months old C1q wild-type (WT) and C1q-deficient (KO) littermate mice were identified and traced in Neurolucida (MBF Bioscience) and dendritic spines were manually identified, counted and quantified as number of spines per μm dendrite length. No significant differences in total spine number per μm dendrite length were detected ($p = 0.47$; $n = 4$ animals/genotype). ***C***, Schematic drawing of the stimulation and recording positions within the dentate gyrus ML. PP, Peforant path; GC, granule cell layer; MF, mossy fibers; SC, Schaffer collaterals. ***D–F***, I/O curves showing the relationship between the presynaptic compound action potential (fiber volley) and the fEPSP in the ML were not significantly different in juvenile (***D***; P14–P17, $p = 0.896$), adult (***E***; 3 months, $p = 0.284$) or aged (***F***; 17-month-old, $p = 0.494$) C1q-deficient (KO) mice, compared with their wild-type (WT) littermates. ***G***, I/O curves showing the relationship between stimulus strength and the fiber volley were not statistically different between juvenile WT and KO mice ($p = 0.86$) but significantly smaller in the adult KO (***H***; $p = 0.05$) and in the aged KO (***I***; $p = 0.0486$), when compared with their respective WT littermates. Juvenile: $n = 6$ WT, $n = 6$ C1q KO littermates; adult: $n = 10$ WT, $n = 12$ C1q KO littermates; aged: $n = 13$ WT, $n = 11$ C1q KO littermates. Values and error bars represent mean ± SEM.

and impacting circuit diversity with aging that is independent of classical complement-activity.

The dramatic increase of C1q in the aging CNS contributes to age-dependent cognitive decline in otherwise healthy subjects

We next investigated whether the accumulation of C1q in the aging brain and its effect on neuronal circuit plasticity in the aging hippocampus functionally contributes to age-dependent cognitive decline. We therefore ran a battery of mouse behavioral tests, known to assess learning and memory functions that involve hippocampal function (Steele and Morris, 1999; Tsetsenis et al., 2011; Mustroph et al., 2012; S. Beraki, L. To, N. L. Saw, M. Priestley, and M. Shamloo, unpublished observations), comparing C1q-deficent mice to their wild-type littermates at 3- and 17-months of age. By comparing the behavioral performance of each age group to a cohort of 3-month-old strain-matched reference mice (3-month-old control) that performed the behavioral tasks identical to 3-month-old C1q wild-type mice (Fig. 9), we were able to assess whether age-dependent cognitive decline occurred in the aged mice tested and whether it was rescued by C1q-deficiency. Interestingly, we did not observe differences between the genotypes at 3 months of age in any of the behavioral tasks analyzed (Fig. 9*A–C* and data not shown). In addition, all of our aged mice were able to learn the standard MWM similar to the 3-month-old control mice (Fig. 9*A′*). Learning of the hidden platform location (days 1–7) was mostly identical between 17-

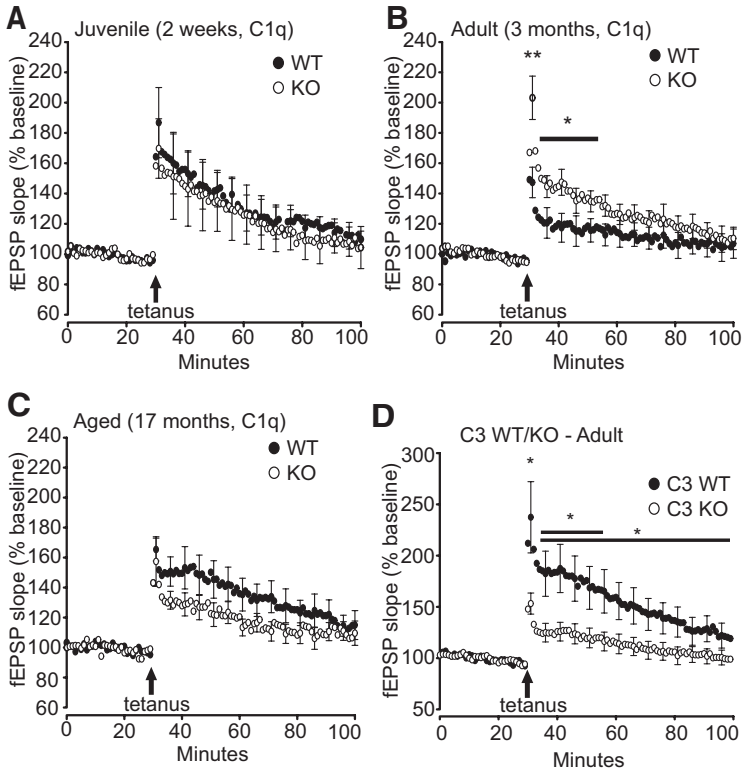

Figure 8. C1q-deficiency enhances activity-dependent synaptic potentiation in the adult, whereas C3-deficiency reduces activity-dependent synaptic potentiation. ***A–C***, Analysis of synaptic potentiation in the ML of juvenile (***A***; P14–P17), adult (***B***; 3-month-old) and aged (***C***; 17-month-old) C1q-deficient (KO) versus WT littermate mice. ***A***, No difference between KO and WT were detected in juvenile mice as synaptic potentiation after tetanic stimulation ($p = 0.867$) was similar between KO and WT mice. ***B***, Adult KO mice showed enhancements in both PTP and subsequent potentiation when compared with the WT (PTP, $p = 0.008$; potentiation after PTP decay, 5–10 min after tetanus, $p = 0.049$; potentiation was significantly different for the time-span from 3 to 20 min post-tetanus, indicated by the bar in the graph, $p = 0.049$). ***C***, No difference between KO and WT were detected in aged mice as synaptic potentiation after tetanic stimulation (PTP, $p = 0.671$, and later potentiation, $p = 0.205$) were similar between KO and WT mice. ***D***, Adult C3-deficient mice (C3 KO) showed an opposing effect to the adult C1q KO (***B***), with reduced PTP and subsequent potentiation when compared with the C3 wild-type littermates (C3 WT; PTP, $p = 0.038$; potentiation after PTP decay, 5–10 min after tetanus, $p = 0.027$; potentiation was significantly different for the entire post-tetanus time-span ($p = 0.044$), including the time-span from 3 to 20 min post-tetanus ($p = 0.029$). Each data point presented represents 1 min averages of four individual fEPSPs taken at 15 s intervals. We did not detect any significant differences between baseline fEPSPs recorded before the tetanic stimulation. Juvenile C1q: $n = 6$ WT, $n = 6$ C1q KO littermates; adult C1q: $n = 10$ WT, $n = 12$ C1q KO littermates; aged C1q: $n = 13$ WT, $n = 11$ C1q KO littermates; adult C3: $n = 14$ WT, $n = 13$ C1q KO littermates. Values and error bars represent mean ± SEM. $^*p < 0.05$, $^{**}p < 0.01$.

and 3-month-old control mice. Only on day 7, the 3-month-old controls performed significantly better than the aged C1q wild-type mice (3-month-old control: 90.29 ± 8.996 s; C1q wild-type: 145.8 ± 15.19 s, $p < 0.01$). However, no significant difference in learning was detected between 3-month-old and aged C1q-deficient mice (126.2 ± 13.48 s, $p > 0.05$). In strong contrast, a reversal learning paradigm of the MWM that is used to assess cognitive flexibility revealed signs of cognitive decline in 17-month-old wild-type littermate mice. Strikingly, old aged C1q-deficient mice performed here similar to the 3-month-old controls, indicating that C1q-deficiency protects from age-related decline in cognitive flexibility (Fig. 9*A′*). On the first day of the reversal learning task (day 8), 3-month-old control mice found the new location of the hidden platform faster than both aged C1q-deficient and C1q wild-type littermate mice (C1q wild-type: 181.0 ± 9.982 s; C1q-deficient: 175.2 ± 9.095 s; 3-month-old control: 129.6 ± 13.94 s; C1q wild-type versus 3-month-old control: $p < 0.05$; C1q-deficient versus 3-month-old control: $p < 0.05$). However, aged C1q-deficient mice performed at the two subsequent reversal learning days as fast as the young controls (day 9: C1q-deficient: 120.8 ± 11.69 s; 3-month-old control: 115.8 ± 13.11, $p > 0.05$; day 10: C1q-deficient: 115.2 ± 11.49; 3-month-old control: 102.7 ± 15.7, $p > 0.05$). This was in strong contrast to the aged C1q wild-type mice which showed reduced reversal learning at both days, consistent with an age-related decline in cognitive flexibility (day 9: C1q wild-type: 171.5 ± 12.13; C1q wild-type vs C1q-deficient: $p < 0.05$; C1q wild-type vs 3-month-old control: $p < 0.05$; day 10: C1q wild-type: 153.0 ± 12.91 s; C1q wild-type vs C1q-deficient: $p > 0.05$; C1q wild-type vs 3-month-old control: $p < 0.05$). This indicates that C1q-deficiency significantly protects from age-related decline in cognitive flexibility. There were no significant differences between the cohorts at all ages during visible platform learning (day 11), indicating that all animals were able to see. In addition, C1q-deficiency also protected from age-dependent decline in spatial working memory as assessed by Y-maze analysis. The degree of cognitive-aging is subject-specific and, accordingly, only approximately half of the aged wild-type littermate mice assessed successfully performed spontaneous alternations in the Y-maze task above chance levels. The other half of aged wild-type littermates, however, revealed age-related decrease in spatial working memory (Fig. 9*B*, circled subjects), reducing total wild-type littermate group performance to chance levels (56.7 ± 3.91%, $p = 0.1158$). In strong contrast, all 17-month-old C1q-deficient mice performed spontaneous alternations in the Y-maze task above chance level and total group performance was significantly above chance (Fig. 9*B*; 64.6 ± 2.83%; $p = 0.0009$), comparable with the 3-month-old controls (Fig. 9*B*; 61.72 ± 3.39%; $p = 0.0072$) and 3-month-old C1q wild-type and C1q-deficient littermate mice (Fig. 9*B*; C1q wild-type: 62.3 ± 2.6%, $p = 0.0004$; C1q-deficient: 61.8 ± 3.5%, $p = 0.0059$). This increased performance in aged C1q-deficient mice was not due to altered activity levels as open field analysis confirmed that C1q-deficient mice have activity levels identical to their C1q wild-type littermates at both 3and 17 months of age (Fig. 9*C*). As to be expected, the 3-month-old control mice traveled slightly longer distance than the old-aged mice (significant difference between aged mice and the 3-month-old controls at 5 min, $p < 0.05$ and 7 min, $p < 0.01$; no significant difference at all other time points; $p > 0.05$). In addition, we did not observe any differences in health, motor function, activity levels, exploratory behavior, or visual abilities, nor did we detect significant differences in anxiety levels at any age (data not shown). Finally, C1q-deficient mice did not show any differences at any age in associative learning compared with their wild-type littermates (data not shown).

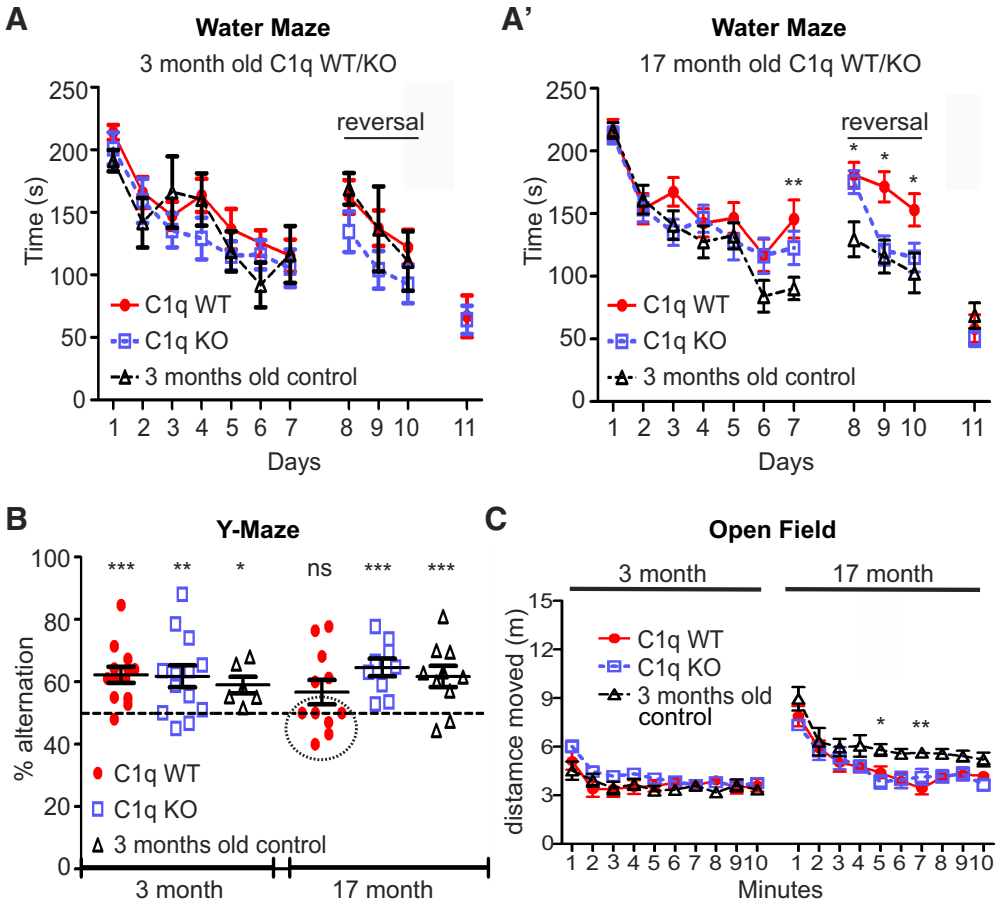

Figure 9. C1q-deficiency reduces cognitive decline during normal aging. ***A***, MWM analysis, including reversal learning (days 8, 9, 10; total escape latency per day shown) revealed enhanced cognitive flexibility in aged C1q-deficient (KO) mice. ***A***, 3-month-old (adult) KO, their WT littermates, and 3-month-old control mice performed all parts of the experiment without significant differences. ***A'***, Learning of the hidden platform location (days 1–7) was nearly identical between 17-month-old (aged) KO mice, their WT littermates and 3-month-old control mice. Only on day 7, the 3-month-old control performed significantly better than the aged WT ($p < 0.01$). However, no significant difference in learning was detected between 3-month-old controls and aged KO mice ($p > 0.05$). On the first day of the reversal learning task (day 8), 3-month-old controls found the new location of the hidden platform faster than both aged KO and WT mice (WT vs 3-month-old control: $p < 0.05$; KO vs 3-month-old control: $p < 0.05$). However, aged KO mice performed at the two subsequent reversal learning days as fast as the 3-month-old controls (day 9: $p > 0.05$; day 10: $p > 0.05$). This was in strong contrast to the aged WT mice which showed reduced reversal learning at both days, consistent with an age-related decline in cognitive flexibility (day 9: WT vs KO: $p < 0.05$; WT vs 3-month-old control: $p < 0.05$; day 10: WT vs KO: $p > 0.05$; WT vs Bio Ctrl: $p < 0.05$). There were no significant differences between the cohorts at all ages during visible platform learning (day 11), indicating that all animals were able to see. ***B***, Y-maze analysis revealed intact spatial working memory in aged KO mice. KO mice performed spontaneous alternations in the Y-maze task at all ages significantly above chance (50%) and equally well as the 3-month-old controls (KO: 3 months of age, $p = 0.0059$; corresponding 3-month-old control, $p = 0.0188$; KO: 17 months of age, $p = 0.0009$; corresponding 3-month-old control, $p = 0.0072$). In contrast, although young adult WT mice were able to learn the task ($p = 0.0004$), a large proportion of aged WT mice did not perform above chance levels (circled subjects), particularly indicating the subjects with age-related decrease in spatial working memory (17-month-old WT, whole group mean: $p = 0.1158$). ***C***, Open field analysis confirmed that KO mice have activity levels identical to the WT at both 3 (adult) and 17 months (aged) of age. As to be expected, the 3-month-old control mice traveled slightly longer distance than the aged KO and WT mice (significant difference between C1qWT/KO and the 3-month-old controls at 5 min: $p < 0.05$, and 7 min: $p < 0.01$; no significant difference at all other time points ($p > 0.05$)). Three-month-old: $n = 13$ WT, $n = 13$ KO littermates; 17-month-old: $n = 11$ WT, $n = 9$ KO littermates; 3-month-old control: $n = 10$; $^{*}p < 0.05$, $^{**}p < 0.01$, $^{***}p < 0.001$. Values and error bars represent mean ± SEM.

These findings show that C1q-deficiency selectively improves distinct cognitive functions particularly in old age.

Discussion

In summary, we have found that C1q levels dramatically increase in close proximity to synapses in the aging brain where it plays a novel role in contributing to aging-dependent cognitive decline. To our knowledge, no protein has ever been demonstrated to increase nearly so dramatically in concert with aging and to accumulate to such a high level in the aging brain. Interestingly, C1q mRNA was previously shown to increase by several-folds in many different mouse tissues with aging, including brain (Zahn et al., 2006; Reichwald et al., 2009; Naito et al., 2012). Our finding that C1q protein levels increased up to 300-fold suggests that the increase with aging is likely due to accumulation of C1q protein released by microglia and inhibitory neurons onto perisynaptic sites. Although our novel finding of C1q protein in a subset of inhibitory neurons in distinct regions of the murine CNS allows for intriguing speculations, we have currently no experimental evidence for functional explanations. However, Simonetti et al. (2013) recently reported that activity-dependent calcium signaling induces the expression of C1q in several neuronal types. Thus, network activity in the mature murine CNS, and in particular specific calcium signaling events in a subset of inhibitory neurons, may drive strong C1q expression which we were able to detect with our novel anti-C1q antibody.

One of the regions that showed the most pronounced increase of C1q protein during CNS maturation and aging in both mice

and humans was the hippocampal dentate gyrus, a region long implicated in age-dependent synaptic changes and cognitive decline in otherwise healthy aged rodents and primates, including humans (Burke and Barnes, 2006; Yankner et al., 2008; Morrison and Baxter, 2012). We were indeed able to show with several behavioral tests that involve hippocampus-dependent function (Steele and Morris, 1999; Tsetsenis et al., 2011; Mustroph et al., 2012; S. Beraki, L. To, N. L. Saw, M. Priestley, and M. Shamloo, unpublished observations) that C1q-deficiency selectively protects from aging-related cognitive decline. Thus, the age-dependent increase of C1q in the CNS correlates with and contributes to the progression of cognitive aging. Interestingly, despite the substantial increase of C1q protein during CNS maturation and an impact of C1q on dentate gyrus-dependent synaptic plasticity in the adult, we did not detect differences between 3-month-old C1q-deficient mice and their wild-type littermates in any of the behavioral tasks performed. This suggests that either only extended C1q accumulation at CNS synapses or the molecular environment in the old aged CNS, together with C1q accumulation, impacts behavioral outcome. Alternatively, our behavioral tasks, optimized to reveal age-dependent cognitive decline, were not suited to detect an impact of C1q on cognition in younger adults. In this regard, our littermate analysis is particularly important, as subtle genetic and environmental differences may have a severe impact on behavioral comparability.

Our data revealed a complex impact of C1q onto synaptic plasticity and the neuronal circuitry in the adult and aging ML, which is independent of the classical complement cascade and not mediated by synapse elimination (Stevens et al., 2007). Indeed, whereas aging-related cognitive decline is known to coincide with synapse loss in the dentate gyrus of otherwise healthy humans and rats (Yankner et al., 2008; Morrison and Baxter, 2012), this aging-dependent synapse loss does not occur in mice (Calhoun et al., 1998). In concordance with our findings, C1q was recently shown to also have noncomplement cascade-dependent modes of action (Benoit and Tenner, 2011; Naito et al., 2012; Nayak et al., 2012; Benoit et al., 2013), and novel roles in synaptic plasticity that are presumably cascade independent have recently been reported for several C1q-like molecules (Matsuda et al., 2010; Uemura et al., 2010; Bolliger et al., 2011). Interestingly, Naito et al. (2012) discovered that C1q promotes aging-associated decline in tissue regeneration in the periphery and that this effect was independent of complement cascade execution but through canonical Wnt signaling. However, whereas C1q augmented Wnt signaling in a variety of tissues, this was not the case for the murine brain (Naito et al., 2012). As such, this suggests that C1q is likely acting via pathways alternative to Wnt for the phenotypes described in the work presented here. Given that we have studied a systemic knock-out of C1q we cannot fully exclude the possibility of a peripheral contribution to the CNS phenotypes described in this study. However, based on our and other labs previously published results that microglia in particular produce C1q protein in the CNS, and our intriguing finding that C1q protein dramatically increases with aging in close proximity to CNS synapses, it is likely that CNS-derived C1q is the source for the physiological changes we have studied and confirmed with this systemic C1q knock-out in otherwise healthy aging mice. Also, as our physiological data confirms that there are no functional abnormalities in the developing C1q knock-out hippocampus; this suggests that the outlined aging-related changes in the hippocampus were not due to altered developmental processes. Important questions for future research, which will be aided by a not yet available conditional C1q knock-out mouse model, will therefore be to understand how C1q impacts the adult and aging circuitry, why C1q accumulates in close proximity to aging synapses, and whether this reflects their senescence.

Finally, our findings have important implications for understanding and treating cognitive decline in the aging CNS and for understanding neurodegenerative diseases, such as Alzheimer's disease. Will drugs that prevent an increase in C1q, or that block its function, lessen cognitive decline, and/or restore cognitive function in normal aging? In addition, it has long been mysterious why the aging CNS has dramatically enhanced vulnerability to neurodegeneration. Our finding that C1q exponentially accumulates at aging synapses may be the missing link as it suggests that these aging synapses are highly vulnerable to any insults that would activate the complement cascade within the CNS. Such insults include CNS ischemia or trauma, systemic bacterial infections, as well as β-amyloid accumulation, which all powerfully activate the complement cascade. Reactive astrocytes triggered by all of these conditions strongly upregulate multiple complement components (Veerhuis et al., 2011; Zamanian et al., 2012). In addition, blood–brain barrier breakdown would allow all serum-borne complement components to flood into the brain, triggering synaptic complement cascade activation, and thus synapse elimination by microglial engulfment (Schafer et al., 2012). Synapse loss is one of the hallmarks of virtually all neurodegenerative diseases (Stephan et al., 2012), by blocking the complement cascade or interfering with the localization of C1q to synapses, it may be possible to prevent this massive synapse loss that drives neurodegeneration in the aging CNS.

References

Benoit ME, Tenner AJ (2011) Complement protein C1q-mediated neuroprotection is correlated with regulation of neuronal gene and microRNA expression. J Neurosci 31:3459–3469. CrossRef Medline

Benoit ME, Hernandez MX, Dinh ML, Benavente F, Vasquez O, Tenner AJ (2013) C1q-induced LRP1B and GPR6 proteins expressed early in Alzheimer disease mouse models, are essential for the C1q-mediated protection against amyloid-beta neurotoxicity. J Biol Chem 288:654–665. CrossRef Medline

Bertholet JY, Crusio WE (1991) Spatial and non-spatial spontaneous alternation and hippocampal mossy fibre distribution in nine inbred mouse strains. Behav Brain Res 43:197–202. CrossRef Medline

Bishop NA, Lu T, Yankner BA (2010) Neural mechanisms of ageing and cognitive decline. Nature 464:529–535. CrossRef Medline

Bolliger MF, Martinelli DC, Südhof TC (2011) The cell-adhesion G-protein-coupled receptor BAI3 is a high-affinity receptor for C1q-like proteins. Proc Natl Acad Sci U S A 108:2534–2539. CrossRef Medline

Botto M, Dell'Agnola C, Bygrave AE, Thompson EM, Cook HT, Petry F, Loos M, Pandolfi PP, Walport MJ (1998) Homozygous C1q deficiency causes glomerulonephritis associated with multiple apoptotic bodies. Nat Genet 19:56–59. CrossRef Medline

Boulanger LM (2009) Immune proteins in brain development and synaptic plasticity. Neuron 64:93–109. CrossRef Medline

Burke SN, Barnes CA (2006) Neural plasticity in the ageing brain. Nat Rev Neurosci 7:30–40. CrossRef Medline

Calhoun ME, Kurth D, Phinney AL, Long JM, Hengemihle J, Mouton PR, Ingram DK, Jucker M (1998) Hippocampal neuron and synaptophysin-positive bouton number in aging C57BL6 mice. Neurobiol Aging 19:599–606. Medline

Drew WG, Miller LL, Baugh EL (1973) Effects of delta9-THC, LSD-25 and scopolamine on continuous, spontaneous alternation in the Y-maze. Psychopharmacologia 32:171–182. CrossRef Medline

Elmer BM, McAllister AK (2012) Major histocompatibility complex class I proteins in brain development and plasticity. Trends Neurosci 35:660–670. CrossRef Medline

Faizi M, Bader PL, Saw N, Nguyen TV, Beraki S, Wyss-Coray T, Longo FM, Shamloo M (2012) Thy1-hAPP(Lond/Swe+) mouse model of Alzheimer's disease displays broad behavioral deficits in sensorimotor, cognitive and social function. Brain Behav 2:142–154. CrossRef Medline

Gerlai R (1998) A new continuous alternation task in T-maze detects hippocampal dysfunction in mice: a strain comparison and lesion study. Behav Brain Res 95:91–101. CrossRef Medline

Hooper N, Fraser C, Stone TW (1996) Effects of purine analogues on spontaneous alternation in mice. Psychopharmacology (Berl) 123:250–257. CrossRef Medline

Hughes RN (2004) The value of spontaneous alternation behavior (SAB) as a test of retention in pharmacological investigations of memory. Neurosci Biobehav Rev 28:497–505. CrossRef Medline

Jacquelin C, Strazielle C, Lalonde R (2012) Spontaneous alternation and spatial learning in Dab1scm (scrambler) mutant mice. Brain Res Bull 87:383–386. CrossRef Medline

Lalonde R (2002) The neurobiological basis of spontaneous alternation. Neurosci Biobehav Rev 26:91–104. CrossRef Medline

Li M, Ager RR, Fraser DA, Tjokro NO, Tenner AJ (2008) Development of a humanized C1q A chain knock-in mouse: assessment of antibody independent beta-amyloid induced complement activation. Mol Immunol 45:3244–3252. CrossRef Medline

Madison DV, Edson EB (2001) Preparation of hippocampal brain slices. Curr Protoc Neurosci 6:64. CrossRef Medline

Matsuda K, Miura E, Miyazaki T, Kakegawa W, Emi K, Narumi S, Fukazawa Y, Ito-Ishida A, Kondo T, Shigemoto R, Watanabe M, Yuzaki M (2010) Cbln1 is a ligand for an orphan glutamate receptor delta2, a bidirectional synapse organizer. Science 328:363–368. CrossRef Medline

Morris R (1984) Developments of a water-maze procedure for studying spatial learning in the rat. J Neurosci Methods 11:47–60. CrossRef Medline

Morrison JH, Baxter MG (2012) The ageing cortical synapse: hallmarks and implications for cognitive decline. Nat Rev Neurosci 13:240–250. CrossRef Medline

Mustroph ML, King MA, Klein RL, Ramirez JJ (2012) Adult-onset focal expression of mutated human tau in the hippocampus impairs spatial working memory of rats. Behav Brain Res 233:141–148. CrossRef Medline

Naito AT, et al. (2012) Complement C1q activates canonical Wnt signaling and promotes aging-related phenotypes. Cell 149:1298–1313. CrossRef Medline

Nayak A, Pednekar L, Reid KB, Kishore U (2012) Complement and non-complement activating functions of C1q: a prototypical innate immune molecule. Innate Immun 18:350–563. CrossRef Medline

Reichwald J, Danner S, Wiederhold KH, Staufenbiel M (2009) Expression of complement system components during aging and amyloid deposition in APP transgenic mice. J Neuroinflammation 6:35. CrossRef Medline

Ricklin D, Hajishengallis G, Yang K, Lambris JD (2010) Complement: a key system for immune surveillance and homeostasis. Nat Immunol 11:785–797. CrossRef Medline

Schafer DP, Lehrman EK, Kautzman AG, Koyama R, Mardinly AR, Yamasaki R, Ransohoff RM, Greenberg ME, Barres BA, Stevens B (2012) Microglia sculpt postnatal neural circuits in an activity and complement-dependent manner. Neuron 74:691–705. CrossRef Medline

Schmid CD, Melchior B, Masek K, Puntambekar SS, Danielson PE, Lo DD, Sutcliffe JG, Carson MJ (2009) Differential gene expression in LPS/IF-Ngamma activated microglia and macrophages: in vitro versus in vivo. J Neurochem 109:117–125. CrossRef Medline

Simonetti M, Hagenston AM, Vardeh D, Freitag HE, Mauceri D, Lu J, Satagopam VP, Schneider R, Costigan M, Bading H, Kuner R (2013) Nuclear calcium signaling in spinal neurons drives a genomic program required for persistent inflammatory pain. Neuron 77:43–57. CrossRef Medline

Steele RJ, Morris RG (1999) Delay-dependent impairment of a matching-to-place task with chronic and intrahippocampal infusion of the NMDA-antagonist D-AP5. Hippocampus 9:118–136. CrossRef Medline

Stephan AH, Barres BA, Stevens B (2012) The complement system: an unexpected role in synaptic pruning during development and disease. Annu Rev Neurosci 35:369–389. CrossRef Medline

Stephan A, Mateos JM, Kozlov SV, Cinelli P, Kistler AD, Hettwer S, Rülicke T, Streit P, Kunz B, Sonderegger P (2008) Neurotrypsin cleaves agrin locally at the synapse. FASEB J 22:1861–1873. CrossRef Medline

Stevens B, Allen NJ, Vazquez LE, Howell GR, Christopherson KS, Nouri N, Micheva KD, Mehalow AK, Huberman AD, Stafford B, Sher A, Litke AM, Lambris JD, Smith SJ, John SW, Barres BA (2007) The classical complement cascade mediates CNS synapse elimination. Cell 131:1164–1178. CrossRef Medline

Tokuyasu KT (1980) Immunochemistry on ultrathin frozen sections. Histochem J 12:381–403. CrossRef Medline

Tsetsenis T, Younts TJ, Chiu CQ, Kaeser PS, Castillo PE, Südhof TC (2011) Rab3B protein is required for long-term depression of hippocampal inhibitory synapses and for normal reversal learning. Proc Natl Acad Sci U S A 108:14300–14305. CrossRef Medline

Uemura T, Lee SJ, Yasumura M, Takeuchi T, Yoshida T, Ra M, Taguchi R, Sakimura K, Mishina M (2010) Trans-synaptic interaction of GluRdelta2 and Neurexin through Cbln1 mediates synapse formation in the cerebellum. Cell 141:1068–1079. CrossRef Medline

Veerhuis R, Nielsen HM, Tenner AJ (2011) Complement in the brain. Mol Immunol 48:1592–1603. CrossRef Medline

Yankner BA, Lu T, Loerch P (2008) The aging brain. Annu Rev Pathol 3:41–66. CrossRef Medline

Zahn JM, Sonu R, Vogel H, Crane E, Mazan-Mamczarz K, Rabkin R, Davis RW, Becker KG, Owen AB, Kim SK (2006) Transcriptional profiling of aging in human muscle reveals a common aging signature. PLoS Genetics 2:e115. CrossRef Medline

Zamanian JL, Xu L, Foo LC, Nouri N, Zhou L, Giffard RG, Barres BA (2012) Genomic analysis of reactive astrogliosis. J Neurosci 32:6391–6410. CrossRef Medline